1971

Surface reactions of boron with clean tungsten substrates

Thomas A. Flaim

1. Boron
I. Title

1C-

SURFACE REACTIONS OF BORON WITH CLEAN TUNGSTEN SUBSTRATES

by

THOMAS ALFRED FLAIM, 1946-

A DISSERTATION

Presented to the Faculty of the Graduate School of the

UNIVERSITY OF MISSOURI - ROLLA

In Partial Fulfillment of the Requirements for the Degree

DOCTOR OF PHILOSOPHY

in

CERAMIC ENGINEERING

1971

P. Darrell Dunnuy
Advisor

Charles Atwell

Raymond F. Vendl

J. Rhoads

C. J. Banick

W. J. James

Publication Option

This dissertation has been prepared in the style utilized by the American Institute of Physics Style Manual. Part I contains the manuscript submitted to Surface Science for publication. Part II contains the manuscript to be submitted to Surface Science for publication in the near future. Appendix I is the manuscript published in the Journal of Vacuum Science and Technology, 8,5(1971)661. Appendices II and III have been added for purposes of clarification.

ABSTRACT

A model developed to predict adsorbate-induced work-function changes for thermionic emitters is shown here to apply to a more general class of electron emission phenomena and a much broader range of adsorbates. This model predicts that chemically, vapor-deposited boron will increase the work function of a clean tungsten substrate at coverages between 0 and 1 monolayer. This is the first time that a single model has been shown to predict both positive and negative work function changes for different adsorbates.

The reactions of chemically, vapor-deposited (CVD) boron with clean tungsten substrates were studied using field emission microscopy (FEM) and low energy electron diffraction (LEED).

The studies by FEM indicate that boron nucleates in the vicinals of and grows across the central tungsten (110) plane. The single-spot, electron emission pattern thus formed is the result of a cap-shaped nucleus of boron which raises the local field strength in the (110) region by decreasing the local radius of curvature. The reversal of the emission characteristic of the clean tungsten (110) plane is not the result of submonolayer adsorption and therefore produces intense, confined electron emission which is independent of adsorption induced work function changes predicted by the general model.

The FEM observations on and around the (100) planes are shown to correlate well with the general model showing a decreased emission (increased work function) with boron adsorption. The LEED study indicates that the CVD boron atoms on a clean tungsten (100) surface occupy epitaxial sites at coverages between 0 and 1 monolayer. These are the same sites that the next layer of tungsten atoms would occupy and represent the simplest potential minima available on the surface.

ACKNOWLEDGEMENTS

The author wishes to thank the staff and students of the Materials Research Center for their valuable discussions and particularly Dr. L. E. Davis for his advice and aid in the pursuit of this problem.

The author would like to thank the members of his committee for their co-operation and constant active participation in his graduate career. Most importantly, the author would like to thank Dr. P. D. Ownby of the Ceramic Engineering Department of the University of Missouri-Rolla, for suggesting the problem and for unfailing confidence and trust throughout this research effort.

TABLE OF CONTENTS

Page

APPENDICES

LIST OF ILLUSTRATIONS

INTRODUCTION

The research reported in this dissertation was accomplished in two parts. The first was a theoretical treatment of adsorbate-induced work function changes with a characterization of the adsorbate-substrate bond and analysis of adsorbate-substrate dipole potential. The second part was a study of surface interactions of chemically, vapor-deposited (CVD) boron with clean tungsten substrates made with Field Emission Microscopy (FEM) and Low Energy Electron Diffraction (LEED).

The theoretical treatment of adsorbate-induced work function changes uses a model originally developed for thermionic emitters and is shown here to apply to field emission, contact potential, and space-charge-limited diode methods of determination of work functions for a very broad range of adsorbates.

This work presents for the first time a single model which predicts both increased and decreased work functions for a substrate depending upon the adsorbate.

A tunnel - resonance approach to electron emission from metal surfaces for alkali adsorption is shown to correlate with the electronegativity model.

The second part of this research project was a study of the surface reactions of CVD boron with clean tungsten substrates using FEM and LEED. The results of the field emission study confirm that boron may nucleate on

the tungsten (110) plane and produce a field emitter with a very small divergence angle for emitted electrons. The LEED study shows that adsorbed CVD boron atoms occupy epitaxial sites on a clean tungsten (100) surface above 650°C.

An application of the general model developed in part one to the changes in electron emission characteristics as observed in the field emission study shows that the increase in work function of this plane is due, at least in part, to the adsorbate-substrate dipole contribution to the total work function as well as a possible local increase in radius of curvature.

PART I

A GENERAL MODEL FOR ADSORBATE-INDUCED WORK FUNCTION CHANGES

ABSTRACT

A simple model for adsorbate-induced work function changes suggested and applied to thermionic emission by Gyftopoulos and Levine[1] is shown to apply generally to field emission, contact potential, space-charge-limited diodes, and retarding potential work function measurement techniques. The general applicability of this theory has evaded theoreticians for a decade as evidenced by the more recent emphasis given in the literature to more sophisticated models which are more difficult to correlate with experimental data. Theoretical data for Li, Na, K, Cs, Th, B, and Si on tungsten are compared to experimental data in the literature and are found to be in good agreement. Variations in values for ϕ_{min} for some systems are related to varying step densities on the field emitters and polycrystalline tungsten substrates, sometimes neglected by experimenters.

INTRODUCTION

The work function of a metallic surface is defined as the minimum amount of energy required to remove an electron from the Fermi level of the metal to the vacuum level. This work function is known to undergo changes in value when an absorbate is deposited onto a clean metal surface. Many have tried to predict these changes in the presence of various absorbates in order to develop a clear understanding of surface-absorbate interactions as they apply to field emission, thermionic emission, and related surface phenomena in general.

A model developed by Gyftopoulos and Levine[1] and applied to thermionic emission will be shown to apply more generally to other work-function, controlled phenomena such as field emission, contact potential, and photo-electrons.

This model treats the adsorbate-induced work function change as a simple sum of a dipole barrier and an electro-negativity barrier.

Gordy and Thomas[2] reported that the work function of a metallic substrate is related to the electronegativity of its constituent atoms by the following relation:

$$\phi = 2.27\ x + 0.34 \text{ e.v.}$$

where ϕ is the work function and x is the relative electro-negativity.[3] The constant term, 0.34 e.v., is the potential due to image forces and is the same for all metals.

The expression $e(\theta)$ for the electronegativity barrier contribution to the work function is derived by assuming the adsorbate to be uniformly distributed over the substrate. When the coverage is zero, the electronegativity of the surface is that of the substrate. Also, the addition of a few atoms does not appreciably change the electronegativity of the surface.[4] The analytical expressions for these two phenomena are:

$$e(\theta)\Big|_{\theta=0} = \phi_m \qquad (1)$$

where ϕ_m = work function of the clean metal

$$\frac{de(\theta)}{d\theta}\Big|_{\theta=0} = 0$$

It is experimentally observed that the work function of the surface covered by one or more monolayers of adsorbate is that of the pure adsorbate, and the addition of absorbate atoms beyond a monolayer does not change the work function.[5]

These two assertions are expressed analytically as:

$$e(\theta)\Big|_{\theta=1} = \phi_f$$

$$\frac{de(\theta)}{d\theta}\Big|_{\theta=1} = 0$$

where ϕ_f is the work function of the absorbate.

An explicit derivation for $e(\theta)$ from first principles

is beyond the present understanding of surface phenomena. However, the function $e(\theta)$ must satisfy the boundary conditions (1) and (2). Thus expanding $e(\theta)$ as a simple polynomial in θ, the expression for $e(\theta)$ is:

$$e(\theta) = \phi_m - (\phi_m - \phi_f)\ (3\theta^2 - 2\theta^3)$$

$$= \phi_f + (\phi_m - \phi_f)\ G(\theta)$$

where $G(\theta) = 1 - 3\theta^2 + 2\theta^3$

Pauling[3] showed that a molecule made of two dissimilar atoms, of relative electronegativities x_1 and x_2 has a dipole moment proportional to the electronegativity difference $(x_1 - x_2)$.

This relationship is confirmed by molecular dipole moment data[3] which show that $M_o = K\ (x_m - x_f)$, where $K = 3.83 \times 10^{-30}$ coul m/v.

This treatment does not consider dipole-dipole interactions. Topping[6] showed that the depolarizing field due to dipoles arranged on a square array is:

$$E(\theta) = 9\ \sigma_f^{3/2}\ \theta^{3/2}\ M(\theta)/4\ \pi\ \varepsilon_o$$

where σ_f = # of sites available for adsorption in a monolayer and $M(\theta) = M_o\ G(\theta)$.

The detailed geometrical arrangement of the adsorbed atoms is not important to this model as variations in geometry give changes in the dipole barrier of the order of 15%.[6]

Allowing for surface mobility of the dipole-dipole interactions, the dipole barrier is:[1]

$$d(\theta) = \frac{-\theta\ G(\theta)\ \sigma_f M_o}{\varepsilon_o\ [1 + 9\alpha\ \sigma_f^{3/2}\ \theta^{3/2}/4\ \pi\ \varepsilon_o]}$$

where α = polarizability of the adsorbate-substrate molecules.

Thus the adsorbate-induced work function change may be expressed as:

$$\begin{aligned} \phi(\theta) &= e(\theta) + d(\theta) \\ &= \phi_f + (\phi_m - \phi_f)\ G(\theta) \\ &\quad - \frac{\theta\ G(\theta)\ \sigma_f M_o}{\varepsilon_o\ [1 + 9\alpha\ \sigma_f^{3/2}\ \theta^{3/2}/4\ \pi\ \varepsilon_o} \end{aligned} \qquad (3)$$

Disregarding detailed geometrical analysis of the adsorbate-substrate bond angles and detailed crystallography of the adsorbate layer, as corrections for these factors are small, it is evident that the expression for $\phi(\theta)$ is most strongly dependent upon θ, the monolayer coverage value and M_o, the isolated substrate-adsorbate dipole moment. The dipole contribution is primarily a result of the electronegativity difference between adsorbate-substrate atoms, as the polarizabilities are usually quite small.

Thus the expression for the work function as a function of coverage is indeed dependent upon the electro-

negativity gradient across the adsorbate-substrate interface.

This model was compared with experimental values of thermionic work function changes due to cesium, strontium, barium, and thorium adsorption on tungsten and molybdenum.[1,5,7,8] The agreement with the thermionic emission data is very good. A comparison of the experimentally determined monolayer coverage value for Cs on tungsten, 4.98×10^{14} Cs atoms/cm^2 to the theoretically determined value of 5×10^{14} Cs atoms/cm^2 for thermionic emitters is remarkable in its agreement.

The present effort is an attempt to extend this model to a treatment of work-function changes due to adsorption as measured by other techniques such as field emission, contact potential, and space charge limited diodes on both single crystal and polycrystalline substrates.

Fowler and Nordheim[9] and Nordheim[10] treated theoretically the emission of electrons from metals in the presence of high fields and the reflection of electrons from a potential barrier which is the sum of a mirror image potential and a linear potential due to an applied electric field.

Using the free electron approximation for describing the metal, they show that the electron current, i, in a one-dimensional system is given by:

$$i = \left(\frac{1.54 \times 10^{10}}{g}\right) \frac{A F^2}{\phi} \exp\left[-0.68 \frac{\phi}{F}^{3/2} f\right]$$

where A is the emitting area, ϕ is the work function (in e.v.), F is the electric field in V/Å , the dimensionless quantities f and g are very slowly varying functions of:

$$X = 3.79 F^{1/2}/\phi$$

which is the fractional change in work function induced by the electric field.[11] The field is related to the applied voltage V and the radius r of the emitter by:

$$F = D V/r$$

Thus, the Fowler-Nordheim equation may be rewritten as:

$$i/V^2 = \alpha \exp\left[-\beta \phi^{3/2}/V\right]$$

The assumption that the adsorbate remains uniformly distributed over the substrate implies β is constant.

A plot of log i/V^2 vs. 1/V gives a slope of $-\beta\phi^{3/2}$. The work function obtained from this treatment is reported to be the work function at 0°K and in the absence of an external field.[12]

This treatment is subject to some limitations when applied to field emitters. In general, the Fowler-Nordheim work function represents a weighted average work function over the whole tip which is made up of many crystal faces. The field emitter tip is usually assumed to have hemispherical

geometry. This geometry requires a finite number of atomic steps to be present on the tip surface, and these steps are involved in an important mechanism in adsorption studies and will be discussed later.

The average work function obtained from Fowler-Nordheim analysis of FEM tips is not a simple arithmetic average of various crystal plane work functions, but in general represents the work function of the most highly emitting region of the tip. In studies made on clean tungsten, this is the region surrounding the (100) pole. Thus, studies of adsorbate-induced work function changes made using the Fowler-Nordheim analysis are highly weighted toward work function changes on the high index regions around the (100) planes.

One of the most interesting adsorbate-substrate systems is that of cesium on tungsten.

As mentioned previously, the earliest study was made by Langmuir and Taylor[5] for thermionic emitters. They report a sharp decrease in the work function of a poly-crystalline tungsten ribbon at low cesium coverages, with the minimum work function being $\sim$ 1.5 e.v. With increasing coverage, the work function slowly rises to the value for metallic cesium, 1.8 e.v. These data were compared with the predictions from the model by Gyftopoulos and Levine.[1] The agreement in terms of monolayer coverage value, and the predictions of work function change vs. coverage are quite good. In particular, the minimum work

function value is lower than either end-member work function and is predicted to be a result of the strong dipole contribution that reduces the total work-function barrier.

Swanson[13] et al. compared work-function data for cesium deposition on tungsten against Langmuir's original data. The agreement is very good and shows that the work-function values obtained by field and thermionic emission are quite consistent. This comparison also indicates that the basic mechanism involved in adsorbate-induced work-function changes must be independent of any particular phenomena inherently characteristic of either thermionic[14] or field emission.[15,16]

Many efforts have been made to explain in detail the interactions involved between substrate and adsorbate atoms. Particular emphasis has been placed on alkali-metal interactions as these systems offer practical applications in devices requiring low-energy plasmas and ion beams.

Following Langmuir's[5] work with cesium on tungsten, the following picture developed. Realizing that the ionization potential of cesium is much lower than that of tungsten, and that the cesium atom is a large atom implies that the cesium atom is adsorbed on a tungsten substrate as an ion. The atom-ion interaction is described by the classical image force. Thus, the resulting system of metal with an absorbed dipole layer that lowers the work function

correlates the experimental data with a reasonable theoretical picture. This point of view has been adopted by DeBoer[17] and more recent efforts by Rasor and Warner,[18] Gadzuk and Carabateas,[19] and MacDonald and Barlow[20] have added sophistications that more closely correlate the theory with experimental data.

Gomer[21] has used this treatment to correlate potassium on tungsten field emission data and found a need for more detailed analysis of the theory.

Gurney[22] originally noted that the interaction of an atom with a metal causes the valence level of the atom to be broadened. This broadening could then cause the formation of polar bonds between adsorbate and substrate which are not necessarily ionic in character.

Gomer and Swanson[23] have provided criteria for establishing the nature of the adsorbate-substrate bond, i.e., whether the bond is ionic, polar, or covalent. Gadzuk[24] has developed a point of view from first principles. Using time-dependent perturbation theory, he finds a broadening of the valence level for alkali atoms adsorbed on metal substrates of about 1 e.v.

Duke and Alferieff[25] treated the substrate-adsorbate interface with a one-dimensional, exactly soluble, pseudo-potential[26] model to calculate the tunneling probability through an adsorbed atom.

Their results indicate that the presence of an atomic energy level in the atom can cause resonance trans-

mission of electrons through the potential barrier when the energy of the tunneling electron is close to the atomic level. Thus, enhanced emission occurs that is not predicted by the Fowler-Nordheim model of field emission. Evidence is offered for zirconium[27] on tungsten and χ-nitrogen[28] on tungsten.

The broadening of the energy levels of the adsorbed atom reported by Gurney[22] is a direct result of the Heisenberg uncertainty principle and the localization of electron states participating in the substrate-adsorbate bonds.

Gadzuk[24] treats the electronic interaction of the adsorbate-substrate atoms with the total Hamiltonian:

$$H_{tot} = H_m + H_a + H_{coup}$$

in which H_m denotes the unperturbed metal, H_a the unperturbed adsorbate atom, and H_{coup} the complete coupling of the atom with the metal.

The electron states associated with the adsorbed atom are broadened to a band width of approximately 1 e.v. In the case of alkali adsorption, the valence states are virtual states. These virtual states are isolated from the states associated with the metal by a potential barrier between the atom and the metal. Even at small separations of the order of a few angstroms, much of this potential barrier remains above the Fermi level. Thus electron states associated with the adsorbate-substrate band are attenuated by this potential. With this model in mind,

the electrons are thought to be tunneling through this barrier. The states on either side of the barrier, the metallic states and the broadened valence states of the adsorbate atoms are exponentially decaying in the barrier region, yet have sufficient overlap to allow significant resonance tunneling between the two types of states.

The position of the adsorbate atom virtual states with respect to the metal Fermi level is very important. At 0°K only those virtual states that lie below the Fermi level of the metal may participate in resonance tunneling through the barrier between the adsorbate atom and the substrate.

In the case of alkali adsorption, where the valence level is much higher than the Fermi level in energy, Gadzuk shows that the expectation value of the population of filled states in the adsorbate virtual band is very close to zero, i.e., very few transitions are expected between the metallic states and the adsorbate states. Very simply, this implies that the alkali atom is chemisorbed as an ion. This is in agreement with the character of the bond predicted from electronegativity arguments.

In addition, Gadzuk goes on to report that as the adsorbate-substrate bond becomes more metallic or covalent in character, the virtual states of the adsorbate atom decrease in energy until, in the case of pure covalent bonding, the virtual states lie below the Fermi level of

the metal. Thus, for covalent or metallic bonding, the virtual states of the adsorbed atom are very nearly full, hence a large number of tunneling events are expected. Again, this agrees with the behavior of electron states associated with adsorbate-substrate bonds from the electronegativity point of view.

It might be pointed out that a correlation of these two points of view implies that the ψ function describing the electron states associated with adsorbate-substrate bonding is an eigen-function of the Hamiltonian describing the adsorbate-substrate interaction, and is indeed sensitive to the difference in energies between the metallic states and the adsorbate valence states. Thus, the treatment developed by Gadzuk parallels the treatment of bond character from the electronegativity point of view developed originally by Pauling.[3]

The concept of resonance tunneling may also be used as an additional point of view to treat gas-phase molecular bond character.

The agreement between field emission and other work-function data of adsorbate-induced, work-function changes implies these changes are accurately described by a Fowler-Nordheim analysis regardless of which point of view is taken to describe the character of the states involved in the adsorbate-substrate interaction (bonding), i.e., the tunnel resonance or electronegativity difference.

Strong evidence[29] exists for the assumption that an electronegativity difference between adsorbate and substrate atoms is one of the key parameters in a theory describing these surface interactions. In studies on field emitters, work function changes due to adsorption may be correlated with electronegativity gradients on the surface and local field effects.[30]

In the present study, data from many sources are correlated with the model based solely on electronegativity gradients and dipole interactions.

A Fortran IV program was written which used the electronegativity values reported by Gordy and Thomas,[2] and the work function data from Michaelson.[47] The program calculated values of $e(\theta)$, $d(\theta)$, and ϕ, the interfacial work function for ten values of coverage between 0 and 1 monolayer. This program repeated these calculations for 200 values of σ_f, the monolayer coverage value in atoms/cm^2.

The closest fit of the theory with the experimental data was determined with the aid of a Wang Model 700 A/B programmable calculator and a nth-order regression analysis numerical program.

ALKALI ADSORPTION

Lithium on Tungsten

In a study of lithium on tungsten, Gavrilyuk and Medvedev[31] measured the work function changes due to

lithium adsorption by Fowler-Nordheim analysis of field emission current-voltage data. In addition to these data, work done by these authors on single-crystal tungsten specimens is reported.[32] A comparison of their reported data with the theoretical treatment from the proposed electronegativity model is shown in Figure 1. They report a value of coverage for ϕ_{min} as 4.2×10^{14} Li atom/cm^2. This value differs from the theoretical value by a factor of 2. Otherwise, the data fit the theory quite well.

Sodium on Tungsten

In a study of sodium adsorption on tungsten, Shrednik and Snezhko[33,34] report the sodium adsorption-induced work function changes on clean tungsten. A comparison of their data with a theoretical curve calculated from the electronegativity model is shown in Figure 2. The theoretical curve is plotted by assuming an average density of sites given by $\sqrt{3}$ times the concentration of sites on the W (100). The theoretical value for monolayer coverage is 3.4×10^{14} Na atoms/cm^2. This compares to a reported value of about 4.0×10^{14} Na atoms/cm^2.

Potassium on Tungsten

The system, potassium on tungsten, has been investigated with field emission by several authors.[35,21] The data from these investigations are plotted against a theoretical curve from the model shown in Figure 3. The

Figure 1. Work function versus coverage for lithium adsorption on tungsten.

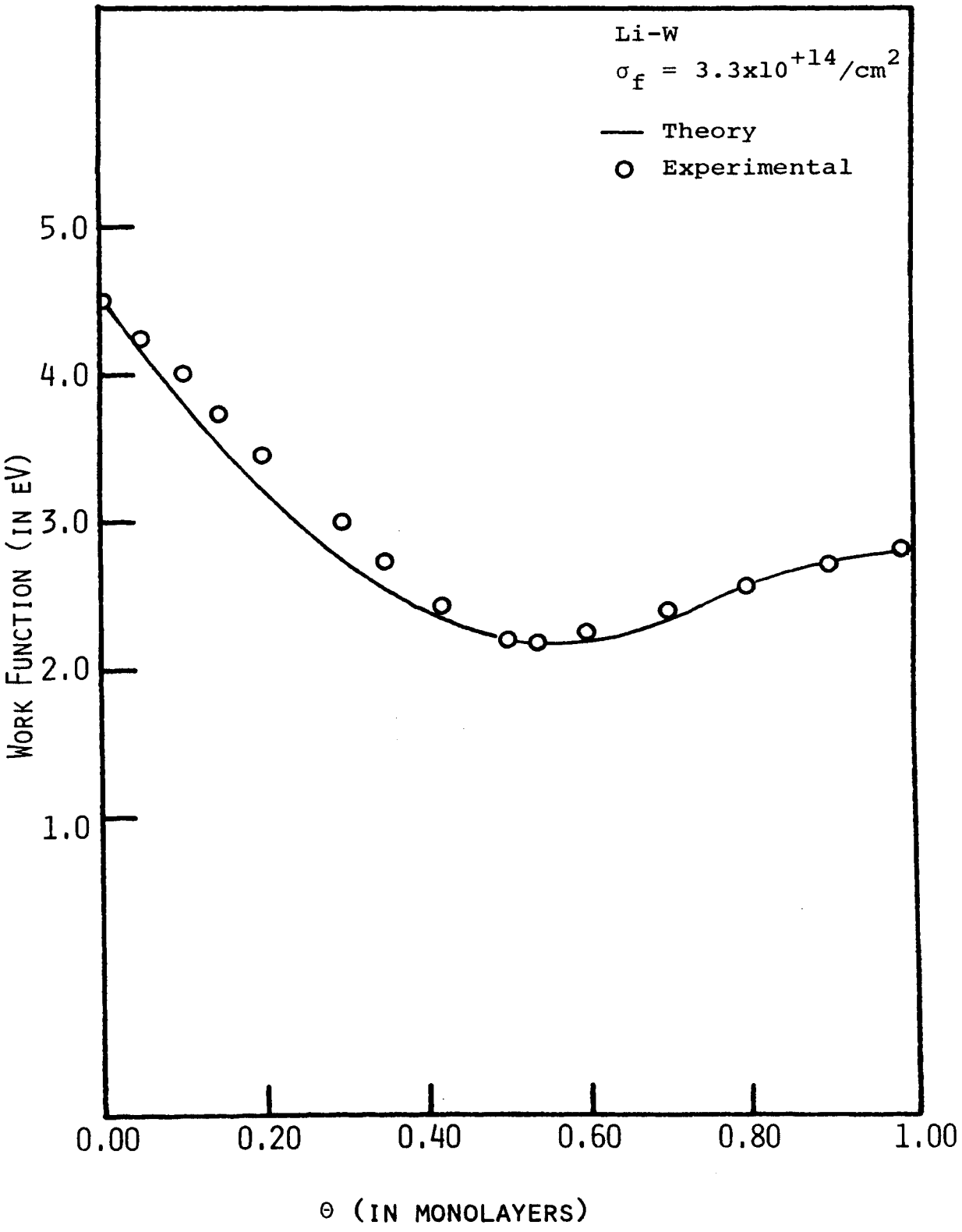
Li-W
$\sigma_f = 3.3 \times 10^{+14}/cm^2$
Theory
Experimental
5.0
4.0
3.0
2.0
1.0
WORK FUNCTION (IN eV)
0.00
0.20
0.40
0.60
0.80
1.00
Θ (IN MONOLAYERS)

FIGURE 1

Figure 2. Work function versus coverage for sodium adsorption on tungsten.

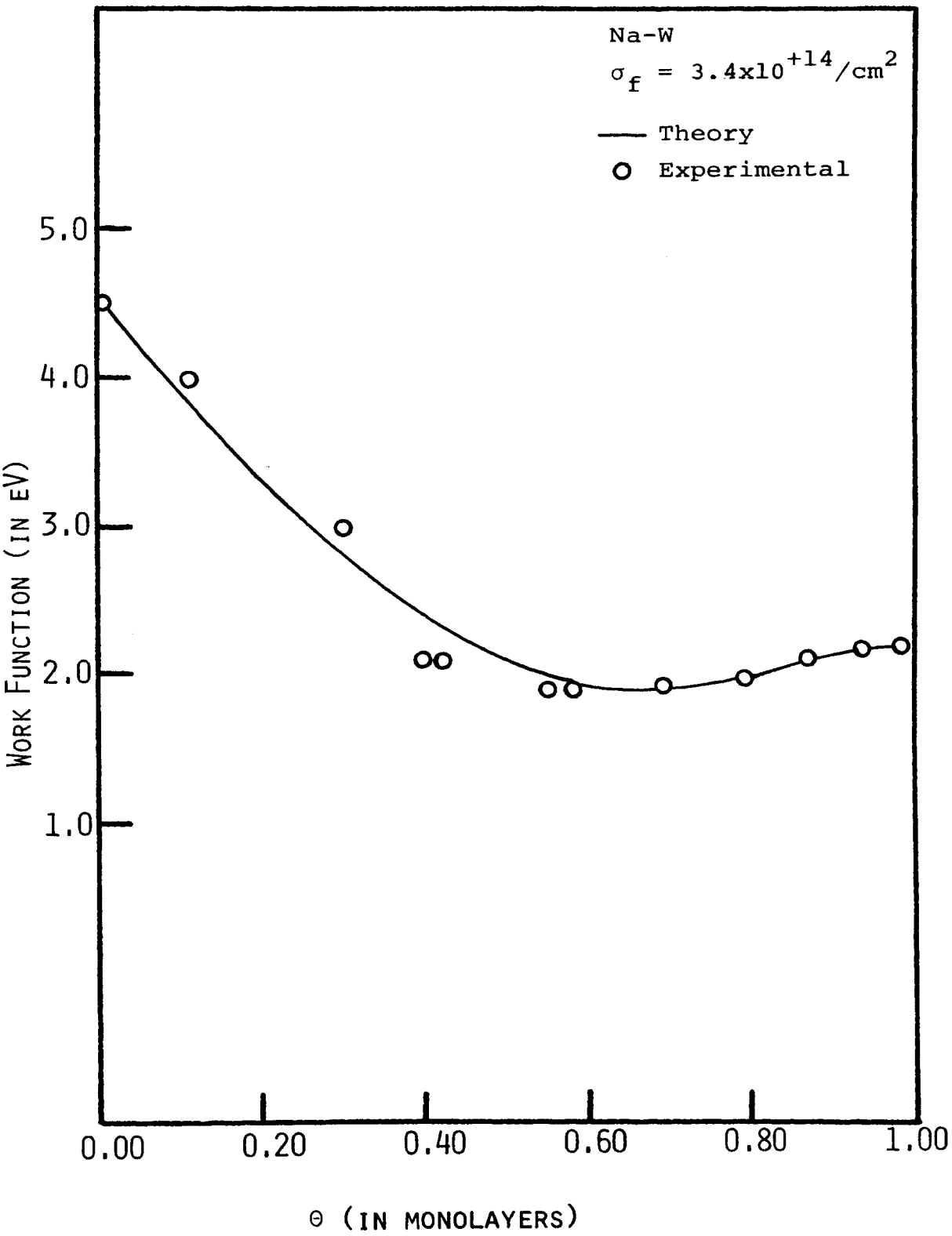
Na-W
$\sigma_f = 3.4 \times 10^{+14}/cm^2$
Theory
Experimental
5.0
4.0
3.0
2.0
1.0
WORK FUNCTION (IN eV)
0.00
0.20
0.40
0.60
0.80
1.00
Θ (IN MONOLAYERS)

FIGURE 2

Figure 3. Work function versus coverage for potassium adsorption on tungsten.

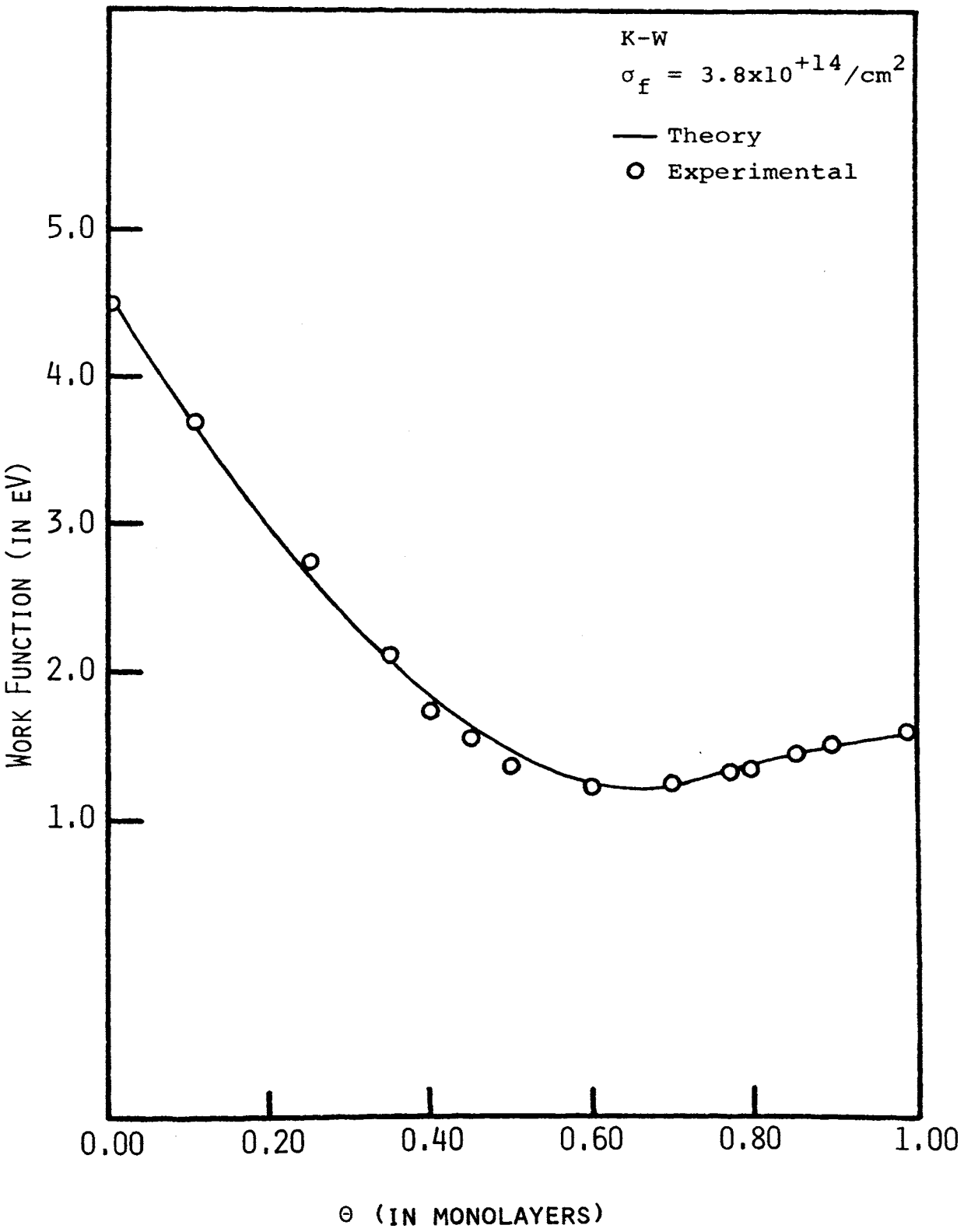
K-W
$\sigma_f = 3.8 \times 10^{+14}/cm^2$
Theory
Experimental
5.0
4.0
3.0
2.0
1.0
WORK FUNCTION (IN eV)
0.00
0.20
0.40
0.60
0.80
1.00
Θ (IN MONOLAYERS)

FIGURE 3

data fit the model very well in both shape and in monolayer coverage. Schmidt and Gomer[21] report that some evidence exists for belief that at about .8 monolayers, some second layer formation begins. This mechanism has not been reported for lithium on tungsten, but has been reported for sodium on tungsten by Chen and Papageorgopoulos.[65] Schmidt and Gomer[21] report a monolayer value of 3.9 x 10^{14} K /cm^2 as compared to a theoretical value of 3.8 x 10^{14} K atoms/cm^2. Ovchinnikov[35] reports no coverage data. An earlier investigation of potassium on tungsten made by Naumovets[36] agrees quite well with the later studies mentioned.

Cesium on Tungsten

In addition to the early study by thermionic emission of cesium deposition on tungsten by Langmuir and Taylor,[5] many more recent efforts have been made using field emission techniques. Studies by Swanson,[37] Fedorus and Naumovets,[38] and Fehrs and Stickney[39] which employed field emission and contact potential measurements were used for comparison with the theory. According to the theory, the minimum work function for Cs/W occurs at approximately 2.8 x 10^{14} Cs atoms/cm^2. This compares to a value of 2.6 x 10^{14} /cm^2 measured by Gavrilyuk[40] et al. and a value of 2.3 x 10^{14} /cm^2 measured by Swanson.[37] A comparison of Swanson's[13] field emission data and the theoretical plot for the W (100) is given in Figure 4. The actual details as to the

Figure 4. Work function versus coverage for cesium adsorption on tungsten.

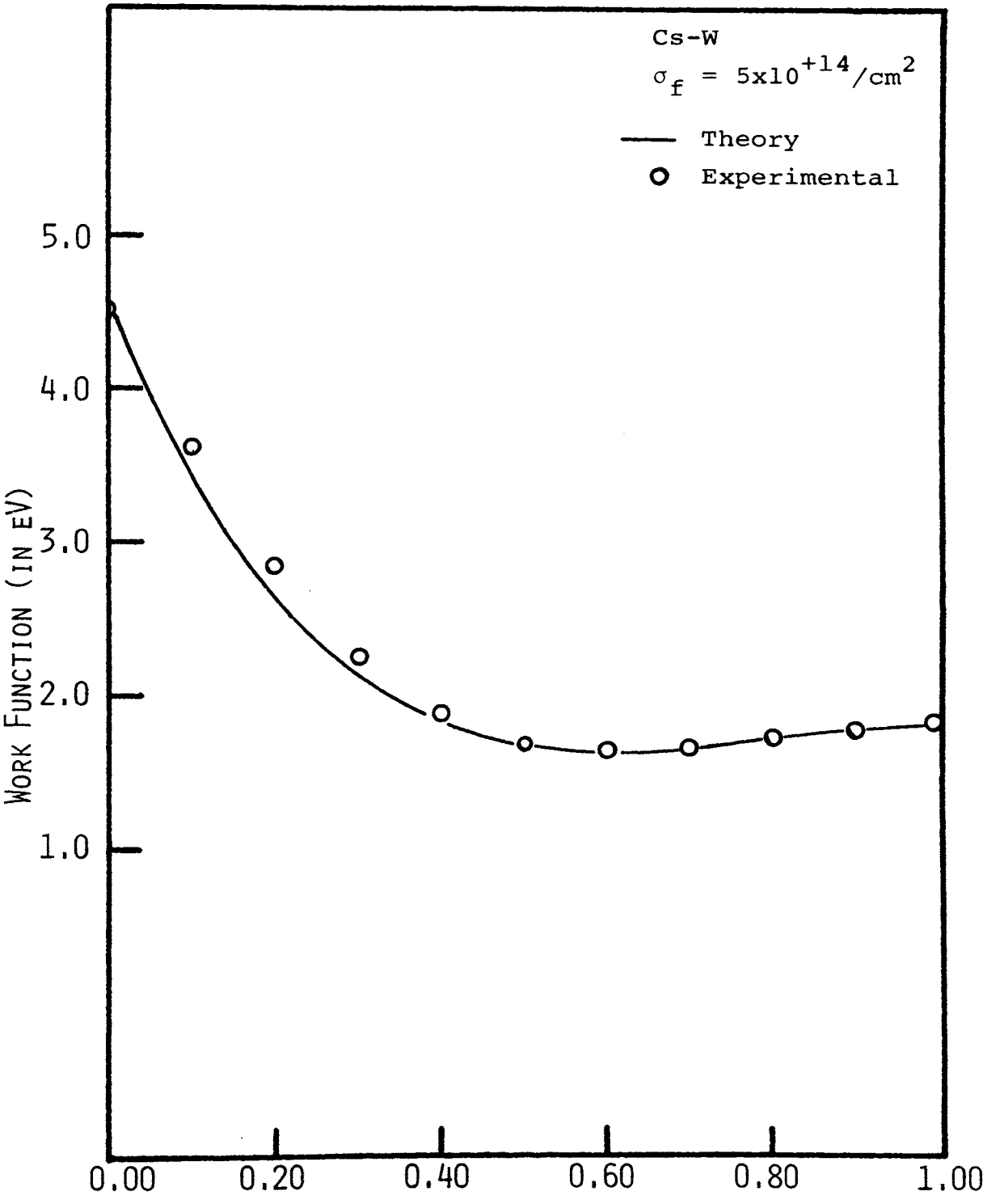
Cs-W
$\sigma_f = 5x10^{+14}/cm^2$
Theory
Experimental
5.0
4.0
3.0
2.0
1.0
WORK FUNCTION (IN eV)
0.00
0.20
0.40
0.60
0.80
1.00
Θ (IN MONOLAYERS)

FIGURE 4

structure of the adsorbed layer of cesium atoms is not completely clear. The theoretically determined value of a monolayer of cesium atoms is 5×10^{14} atoms/cm^2. This is in good agreement with published values.

In their recent paper, Fehrs and Stickney[39] studied the adsorption of Cs and K on Ta (110) and W (100). In their study by contact potential methods, they show that surface migration of cesium begins at 1×10^{14} Cs atoms/cm^2 at $T_s > 300°K$, where T_s is equal to the temperature of the substrate. Thus their reported $\Delta\phi$ vs. n curve is shifted to the right, and their coverage data are somewhat less than ideal. The authors report that at the low coverage limit, i.e. $n \to 0$, the slope of the plot $\Delta\phi$ vs. n is related to the low-coverage, dipole moment of the adsorbate-substrate bond by:[42,43]

$$\mu = \frac{C}{2\pi} \left[\frac{2(\Delta\phi)}{2n}\right]_{n\to 0}$$

where $C = 1/300$ when the units of μ_o, $\Delta\phi$, and n are respectively Debye (1×10^{-18} esu), electron volts, and atoms/cm^2. Also, they point out that the monolayer coverage value is determined by the point where the ϕ vs. n curve reaches the value of ϕ_f, the work function of the adsorbate. These two concepts are in agreement with this model, and are discussed in a later section.

POLYVALENT ADSORBATES

Thorium on Tungsten

Investigations of thorium on tungsten have been made

by thermionic[44] emission, LEED and Auger emission spectroscopy.[45]

The results of the thermionic emission study by Estrup[44] et al. are compared to the theoretical curve computed for the W (100) (Figure 5). The agreement, in general, is quite good.

Any discrepancy here may be due to either an erroneous value for $\sigma_f \sim 8 \times 10^{14}$ atoms/cm^2 or the surface may have been contaminated by ambient gases. The actual value of σ_f determined experimentally is somewhat in question. Using the criteria of Fehrs and Stickney,[39] the determination of σ_f from thermionic emission measurements is quite difficult. The problem may lie in the fact that no data exist for work functions of single crystal planes of thorium. Estrup[44] et al. report LEED evidence for the formation of epitaxial layers of thorium on tungsten. Retarding potential measurements by the same authors were in good agreement with the thermionic emission data.

Pollard[45] made a correlated study by LEED, Auger, and work-function measurements of the thorium on tungsten system by the retarding-potential method. Pollard correlates the growth of the 64 e.v. Auger peak of thorium with the coverage.

The point where the height of the Auger peak reaches the first maximum is defined as the coverage corresponding to one monolayer. This differs from

Figure 5. Work function versus coverage for thorium adsorption on tungsten.

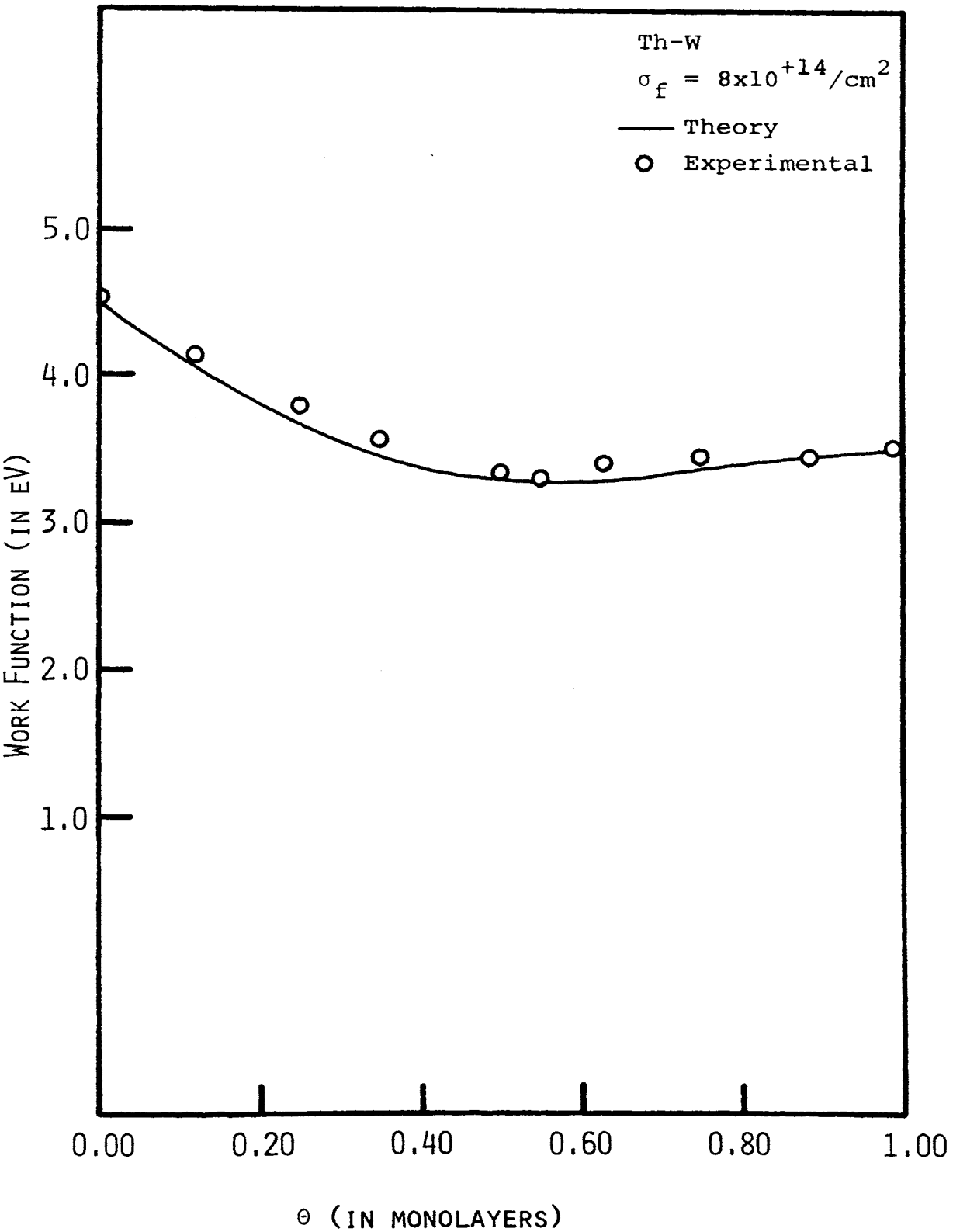
Th-W
$\sigma_f = 8x10^{+14}/cm^2$
Theory
Experimental
5.0
4.0
3.0
2.0
1.0
WORK FUNCTION (IN eV)
0.00
0.20
0.40
0.60
0.80
1.00
Θ (IN MONOLAYERS)

FIGURE 5

the value predicted by work function measurements by approximately 30%. This discrepancy may be due to the structure of the thorium overlayer, or the formation of a second layer at approximately 0.8 monolayer.

Silicon on Tungsten

Using field emission techniques and Fowler-Nordheim analysis of work functions, Collins[46] has made a study of silicon adsorption on tungsten.

The change in the Fowler-Nordheim pre-exponential term is given and is found to vary only slightly over the range from 0 → 1 monolayer. The results of this study are plotted against a theoretical curve predicted from electronegativity values (Figure 6). The agreement is exceptionally good and represents strong evidence for the validity of the theoretical model. Other models have failed to predict increases in work function with adsorption and here for the first time a single model is shown to accurately predict both positive and negative work function changes from zero to one monolayer coverage. The theoretically predicted value for σ_f, i.e., the monolayer number of silicon atoms on tungsten field emitters is 2.0×10^{15} Si atoms/cm^2. Unfortunately, Collins does not report absolute values for coverages so they cannot be correlated.

Figure 6. Work function versus coverage for silicon adsorption on tungsten.

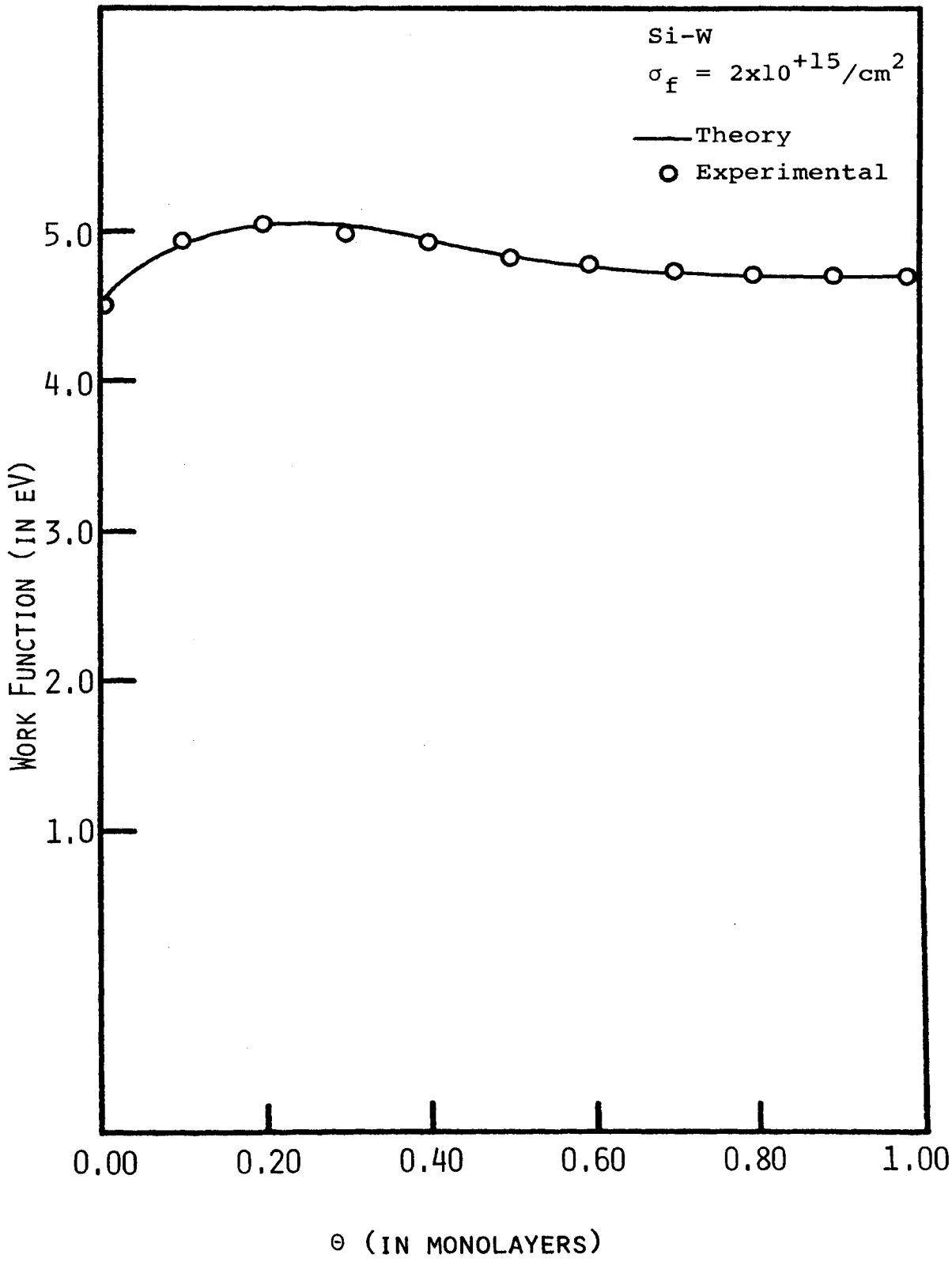
Si-W
$\sigma_f = 2x10^{+15}/cm^2$
Theory
Experimental
5.0
4.0
3.0
2.0
1.0
WORK FUNCTION (IN eV)
0.00
0.20
0.40
0.60
0.80
1.00
Θ (IN MONOLAYERS)

FIGURE 6

Boron on Tungsten

Young[66] studied work function changes on clean tungsten field emitters due to boron adsorption. A comparison of his experimental data with the theoretical curve is shown in Figure 7. The coverages reported by Young are somewhat questionable, but a comparison of the theoretically calculated σ_f value of 2.3×10^{15} atoms/cm^2 agrees quite well with the value 2.2×10^{15} atoms/cm^2 obtained by the present authors from the criteria described in Part II.

DISCUSSION AND CONCLUSIONS

A detailed numerical study of the behavior of eq. 3 was made. The behavior of this equation is such that the most important variable is σ_f, the number of sites available for absorption in one monolayer. This strong dependence upon the monolayer coverage value, σ_f, of the work function change due to adsorption is a useful property. The value of σ_f is dependent upon the substrate lattice parameter, surface structure, and step density.[1] The variation in σ_f with step density has been shown previously.[48] In particular, for boron adsorption on tungsten field emitter tips, step densities contribute 50% of the sites available for adsorption. In general, the importance of step densities will be dependent upon the adsorbate involved. For field emitter tips, the step density is expected to increase with decreasing tip radius. The

Figure 7. Work function versus coverage for boron adsorption on tungsten.

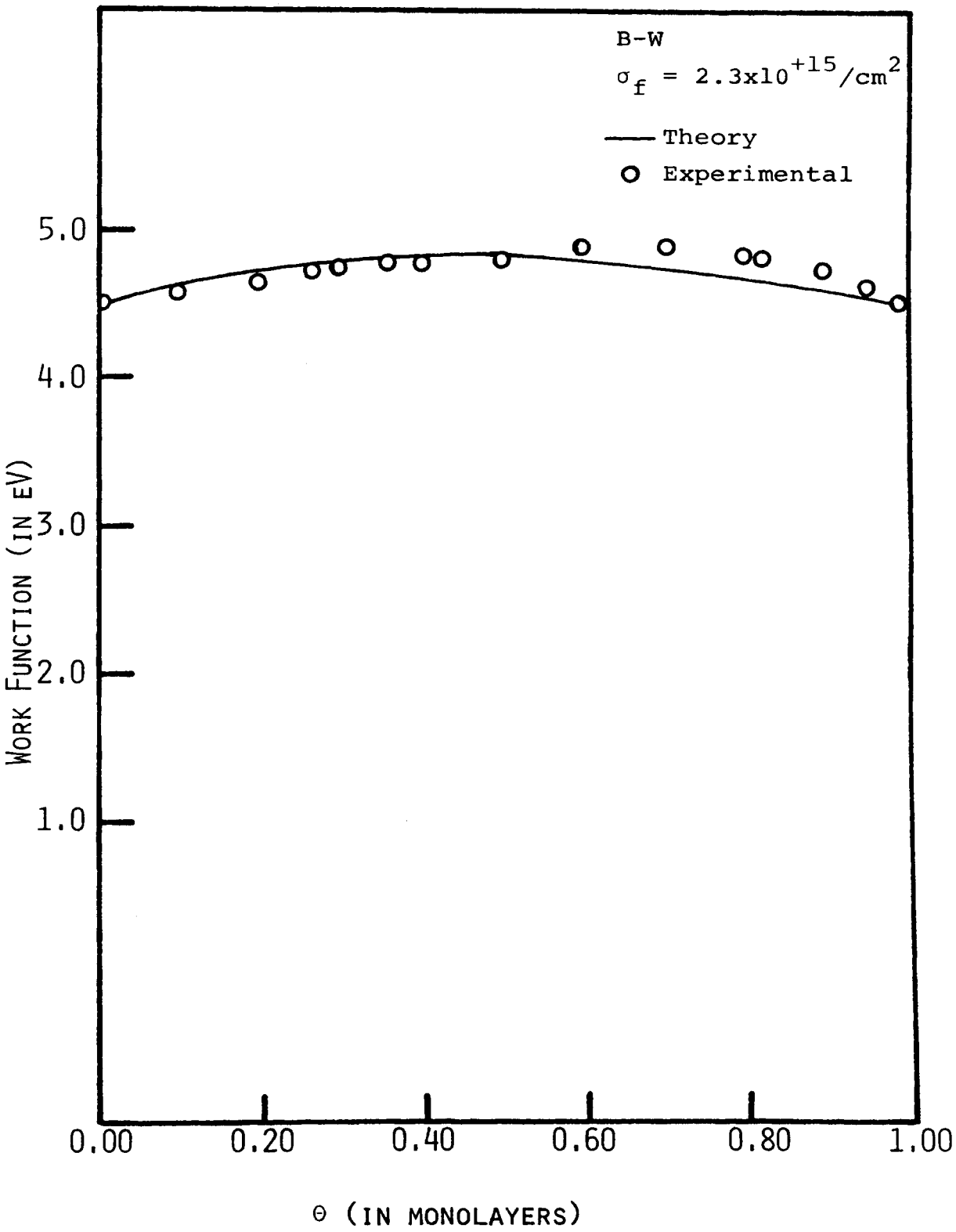
B-W
$\sigma_f = 2.3 \times 10^{+15}/cm^2$
Theory
Experimental
5.0
4.0
3.0
2.0
1.0
WORK FUNCTION (IN eV)
0.00
0.20
0.40
0.60
0.80
1.00
Θ (IN MONOLAYERS)

FIGURE 7

explicit dependence of step density on tip radius is being studied. However, most authors neglect to report this important parameter in studies made by field emission techniques.

In general, a change in σ_f of the order of 10% will change the value of ϕ_{min} by $\sim$ 20%, and will change the fractional value of θ at which ϕ_{min} occurs. Thus slight variations in step density over a field emitter tip may very well be responsible for variations in ϕ_{min} and σ_f reported for such systems as Cs/W.

The theoretical model is dependent upon the clean substrate work function, substrate electronegativity, and lattice parameter, but is not an explicit function of the substrate surface structure. The model is also dependent upon adsorbate electronegativity, covalent radius, and the absorbate work function; but is independent of adsorbate structure except where large differences exist in work function values for different crystal planes of the adsorbate.

The Case for Nitrogen

Nitrogen adsorption on tungsten has been studied by many techniques; flash desorption, field emission, LEED, and Auger among others.

Nitrogen is somewhat unique in that it can lower the work function of clean tungsten in spite of the fact that atomic nitrogen has an electronegativity of 3.0.[2]

The idea that molecular gases may bond to a surface with more than one discrete binding energy is not new. Multiple binding states are used to rationalize apparently anomalous work function changes at high surface concentrations.[49]

Early studies of the interaction of nitrogen with tungsten by flash desorption[50] identified three different chemisorbed states. Two of these appear at room temperature. The first is a weakly bound state α. The α state forms concomitantly with the second more energetic β state. The α state has a binding energy of $\sim$ 20 Kcal/mole. The α state apparently forms primarily on the region along the (111) zone.

The β state was found to desorb in a second order reaction, implying this state is atomic, with an activation energy of 81 Kcal/mole.[51] Verification of the atomic nature of the β state was offered by Kislivk.[52] Late workers have measured the β state binding energy as 85 Kcal/mole[53] and 87 Kcal/mole.[54]

A third state γ was identified at temperatures below 150°K.[55] Field emission measurements[56] confirmed the existence of this third state. At room temperature, the work function was lowered.

In more recent efforts using flash desorption mass spectrometry, Clavenna and Schmidt[57] report three binding states on the tungsten (100) over a broad temperature

range. However, Germer and Adams[58] using flash desorption mass spectrometry and LEED report only one binding state for nitrogen adsorption on the W (100).

Further investigations have reported other binding states, which are a result of electron impacted γ-nitrogen.[59, 27,28]

The treatment of nitrogen adsorption on tungsten is being carried out in this laboratory. Results are to be published later for this system as well as others.

In general, however, the work of Hayes et al.[60] using space-charge-limited and retarding-field diodes to measure work function changes of tungsten due to nitrogen adsorption confirms the theoretical model qualitatively.

The $\Delta\phi$ vs. coverage curves reported are in good agreement with those predicted by the model if the adsorbed species has an electronegativity very slightly less than that of clean tungsten. This may be the case if the adsorbate has bonding between nitrogen atoms as well as bonding to the substrate. This model of "quasi-chemisorbed" nitrogen is a bonding scheme present in some organic molecules, particularly the azides.[61] Until a better understanding of adsorption of molecular gases is available, the authors are provisionally accepting this model as correct.

Hayes et al. points out several results that are particularly interesting. Their study shows that any work function change will depend upon:

1) The relative rates of adsorption onto the different sites.
2) The magnitude of the absolute work functions of the individual crystallographic planes both for the clean and the gas-covered surfaces.
3) The fractional contribution to the total surface area of each type of plane.

These results are in good agreement with the conclusions reached when the model dependence upon these substrate parameters was studied.

Other experimental work by Holscher[62] and Oguri[63] indicates that the magnitude and the sign of the work function change are dependent upon crystallographic orientation.

Recent work by Sargood[64] et al. has shown that electronegativity is dependent upon crystallographic orientation and they report a linear relationship between experimentally determined absolute electronegativities and work function for clean tungsten substrates.

These data, coupled with the good agreement between the experimentally determined work function changes and theoretical predictions from electronegativity differences that fit this model plus its applicability to thermionic, field emission, and other methods of measuring work function thanges due to adsorption, indicate a much broader range of pertinence than has previously been recognized.

The predictions that are a result of the numerical

study of the behavior of this model indicate that differences previously reported for ϕ_{min}, σ_f, and ϕ_f may be a natural result of the differences in substrates, particularly for field emission studies, as was predicted by Hayes[60] from experimental data.

In general the phenomena responsible for the work function change vs. coverage may be summarized as follows:

1) At the low coverage limit $\theta \rightarrow 0$, the initial rapid change in the work function is related to the strong effect isolated dipoles have on the work-function potential barrier. The dipole moment may be calculated from:[39]

$$\mu_o = \frac{C}{2\pi} \left[\frac{2(\Delta\phi)}{2n}\right]_{n\rightarrow 0}$$

2) Behavior in the region of the work function vs. coverage plot where:

$$\frac{d\phi}{d\theta} = 0$$

is due to the fact that as the coverage is increased, the dipoles begin to interact much more strongly with each other, with a depolarizing field given by:[1]

$$E(\theta) = 9\ \sigma_f^{3/2}\ \theta^{3/2}\ M(\theta)/4\pi\varepsilon_o$$

At $\frac{d\phi}{d\theta} = 0$ the coverage has reached a value such

that the addition of more adsorbate atoms gives rise to more depolarizing effects than it does to producing polarizing dipoles. Hence, the slope of the ϕ vs. θ curve changes sign.

3) At high coverages, $\theta \rightarrow 1$, the surface becomes more nearly like that of a pure adsorbate surface, and the work function approaches that of the adsorbate.[38]

The dependence of σ_f upon step density calls for more authors reporting tip radii when making field emission studies, and an urgent need for more investigations to report coverage data in absolute values rather than arbitrary units.

ACKNOWLEDGEMENTS

We would like to thank the staff of the University of Missouri-Rolla Computer Science Center for their help in processing the programs.

REFERENCES

1. E. P. Gyftopoulos and J. D. Levine, J. Ap. Phys., 33 (1962) 67.

2. W. Gordy and W. J. Thomas, J. Chem. Phys., 24 (1956) 439.

3. L. Pauling, The Nature of the Chemical Bond (Cornell University Press, Ithaca, New York, 1960) Third Edition.

4. G. Ehrlich, Structure and Properties of Thin Films, edited by C. A. Neugebaur, J. B. Newkirk, and D. A. Vermilyea (John Wiley and Sons, Inc., New York, 1959).

5. I Langmuir and J. B. Taylor, Phys. Rev., 44 (1933) 423.

6. J. Topping, Proc. Roy. Soc. (London) A114 (1927) 67.

7. G. F. Moore and H. W. Allison, J. Chem. Phys., 23 (1955) 1609.

8. W. Bratton and J. Becker, Phys. Rev., 56 (1939) 947.

9. R. H. Fowler and L. Nordheim, Proc. Roy. Soc. (London) A119 (1928) 173.

10. L. Nordheim, Proc. Roy. Soc. (London), A121 (1928) 626.

11. R. E. Burgess and H. Kroemer, Phys. Rev., 90 (1953) 515.

12. G. Ehrlich, Advances in Catalysis, 14 (1963) 255.

13. L. W. Swanson, R. W. Strayer, C. J. Bennette, and E. C. Cooper, NASA Contract #NAS3-2596 final report, NASA document #CR-54106, (1964).

14. C. Herring, Rev. of Mod. Phys., 21 (1949) 185.

15. R. H. Good and E. W. Muller, Handbuch der Physik, 21 (1956) 176.

16. R. Gomer , Field Emission and Field Ionization, Harvard University Press, Cambridge (1961).

17. J. H. DeBoer, Advances in Catalysis, Vol. VIII (Academic Press, Inc., New York, 1956).

18. N. S. Rasor and C. Warner, J. Appl. Phys., 35 (1964) 2589.

19. J. W. Gadzuk and E. N. Carabateas, J. Appl. Phys., 36 (1965) 357.

20. J. R. MacDonald and C. D. Barlow, J. Chem. Phys., 40 (1964) 1535; 43 (1965) 2572; 44 (1966) 202.

21. L. Schmidt and R. Gomer , J. Chem. Phys., 42 (1965) 3573.

22. R. W. Gurney, Phys. Rev., 47 (1935) 479.

23. R. Gomer and L. W. Swanson, J. Chem. Phys., 38 (1963) 1613.

24. J. W. Gadzuk, Surf. Sci., 6 (1967) 133; Surf. Sci., 6 (1966) 159.

25. C. B. Duke and M. E. Alferieff, J. Chem. Phys., 46 (1967) 923.

26. W. A. Harrison, Pseudopotentials in the Theory of Metals, (W. A. Benjamin, Inc., New York, 1966).

27. E. W. Plummer, J. W. Gadzuk, and R. D. Young, Solid State Commun., 7 (1969) 487.

28. W. Ermich and A. VanOostrom, Solid State Commun., 5 (1967) 471.

29. A. J. Sargood, C. W. Jowett, and B. J. Hopkins, Surf. Sci., 22 (1970) 343.

30. F. Ashworth, Advances in Electronics, 3 (1951) 1.

31. V. M. Gavrilyuk and V. K. Medvedev, Sov. Phys.-Solid State, 8 (1966) 1439.

32. V. M. Gavrilyuk and V. K. Medvedev, Soviet Physics-Solid State, 6 (1964) 2727.

33. V. N. Shrednik and E. V. Snezhko, Soviet Physics, 6 (1965) 2727.

34. N. V. Shrednik and E. V. Snezhko, Soviet Physics, 6 (1964) 1173.

35. A. P. Ovchinnikov, Soviet Physics-Solid State, 9 (1967) 483.

36. A. G. Naumovets, Soviet Physics-Solid State, 5 (1963) 1668.

37. L. W. Swanson and R. W. Strayer, J. Chem. Phys., 48 (1968) 2421.

38. A. G. Fedorus and A. G. Naumovets, Surf. Sci., 21 (1971) 426.

39. D. L. Fehrs and R. E. Stickney, Surf. Sci., 24 (1971) 309.

40. V. M. Gavrilyuk, A. G. Naumovets, and A. G. Fedorus, Zh. Eksper, i Theor. Fiz., (1966) 1332.

41. A. G. Naumovets, and A. G. Fedorus, Fiz. Tverd. Tela., 10 (1968) 801.

42. I. Langmuir, J. Am. Chem. Soc., 54 (1932) 2798.

43. J. H. DeBoer, Electron Emission and Adsorption Phenomena, (Cambridge University Press, London 1935).

44. P. J. Estrup, J. Anderson, and W. E. Danforth, Surf. Sci., 4 (1966) 286.

45. J. H. Pollard, Surf. Sci., 20 (1970) 269.

46. R. A. Collins, Surf. Sci., 26 (1971) 624.

47. H. B. Michaelson, J. Appl. Phys. 21 (1950) 536.

48. T. A. Flaim and P. D. Ownby, NSF Final Report, Contract #GK 4625 (1971).

49. G. Ehrlich, Structure and Properties of Thin Films, 423, (C. A. Neugebauer, J. B. Newkirk, and D. A. Vermilyea, Eds., Wiley, New York, 1959).

50. G. Ehrlich, J. Phys. Chem., 60 (1956) 1388.

51. T. W. Hickmott and G. Ehrlich, J. Phys. Chem. Solids, 5 (1958) 47.

52. P. Kislivk, J. Chem. Phys., 30 (1959) 174.

53. P. Kislivk, J. Chem. Phys., 31 (1959) 1605.

54. R. A. Redhead, Vacuum, 12 (1962) 203.

55. G. Ehrlich, J. Chem. Phys., 34 (1961) 29.

56. G. Ehrlich and F. G. Hudda, J. Chem. Phys., 35 (1961) 1421.

57. L. R. Clavenna and L. D. Schmidt, Surf. Sci., 22 (1970) 365.

58. D. L. Adams and L. H. Germer, Surf. Sci., 26 (1971) 109.

59. J. T. Yates and T. E. Madley, Nuovo Cimento Suppl., 5 (1967) 59.

60. F. H. Hayes, M. P. Hill, S. M. A. Lecchini, and B. A. Pethica, J. Chem. Phys., 42 (1965) 2919.

61. R. Q. Brewster, Organic Chemistry, (Prentice-Hall, Englewood Cliffs, New Jersey, 1953).

62. A. A. Holscher, J. Chem. Phys., 41 (1964) 571.

63. T. Oguri, J. Phys. Soc., (Japan), 19 (1964) 83.

64. A. J. Sargood, C. W. Joulett, and B. J. Hopkins, Surf. Sci. 22 (1970) 343.

65. J. M. Chen and C. A. Papageorgopoulos, Surf. Sci., 21 (1970) 377.

66. R. D. Young, Contract Number AFOSR-TN-56-317, ASTA Document Number 94853 (1956).

PART II

SURFACE REACTIONS OF CHEMICALLY VAPOR DEPOSITED BORON WITH CLEAN TUNGSTEN SUBSTRATES

INTRODUCTION

The surface reactions of chemically-vapor-deposited (CVD) boron with clean tungsten substrates was studied by Field Emission Microscopy (FEM) and Low Energy Electron Diffraction (LEED).

Previous studies of boron reactions with tungsten substrates have been made with FEM by Young[1] and with LEED by Tucker.[2] Both of these studies used physically, vapor-deposited of elemental boron from heated rods of boron as adsorbate sources. Both studies suffer from a lack of ability to determine the number of adsorbed atoms deposited. This study was made in an effort to improve upon deposition technique and to study surface reactions between boron and tungsten at known coverages below one monolayer using both FEM and LEED together.

Boron tri-iodide (BI_3) was used in a more recent study of boron reactions with clean tungsten by field emission techniques.[3] Monomeric BI_3 molecules were observed to be the principal vapor species to sublimate into an ultra-high vacuum environment at room temperature.[4] No polymers were observed in the vapor. The choice of BI_3 as a source material for studying boron reactions with tungsten was also influenced by the fact that iodine can be easily pumped without damage to the vacuum system.

Changes in electron emission characteristics of specific crystallographic surfaces on field emitter tips may be caused by several possible phenomena:

1) The adsorbate may change the work function of the specific plane, and yet may or may not participate in any particular change in the substrate surface structure of that plane.

2) Adsorbate may nucleate forming a three-dimensional protuberance of a much smaller radius than that of the tip and therefore enchance electron emission due to the local increase in electric field.

3) Adsorbed species which are smaller than the substrate atoms may fit into steps or surface interstices effectively smoothing an irregular (although atomically flat) surface thereby decreasing the electron emission by increasing the local radius.

4) Good and Muller[5] discussed a mechanism whereby an adsorbate non-metal can increase field electron emission by electronic interaction in which the empty conduction band of an adsorbed semiconductor or insulator provides a reservoir for electrons which have tunneled through this interface. The two thin barriers which must be penetrated in this case are considerably thinner than the single one present for the clean metal surface.

Several review articles on LEED[6,7,8,9] are available in the literature and the reader is referred to these for discussions of the concepts involved in this technique. Appendix III is a discussion of the two-dimensional reciprocal lattice.

The unambiguous interpretation of LEED patterns, i.e. identification of the unit cell, measurement of cell parameters, and the location of all atoms within the unit cell, is still an unaccomplished objective.[10]

Many authors[11-19] have tried various approaches, but in general, only qualitative data are to be obtained until a better understanding of the diffraction process is known.

Reasonable success has been made in interpretation of LEED patterns from clean metals such as nickel[7,8,9] and tungsten[6,20-23] but surface structures of materials such as silicon and germanium[24,25,26] present many problems.

Lander[27] has reported that a surface layer with slightly larger or smaller cell parameters than that of lower lying layers will give rise to fractional-order spots in a LEED pattern. This lattice parameter shift in the surface layer has been reported by MacRae[7] for nickel. The nickel surface layer is reported to have an approximately 5% larger cell parameter than that of underlying layers. This expanded layer is referred to as the substrate selvedge by Wood.[28] This selvedge structure may be related to the structure of a parallel planar section of the substrate material by small displacements of atoms.[27] This displacement in the selvedge then is responsible for fractional order spots observed in clean surface LEED patterns.

The sensitivity of LEED patterns to surface cleanliness has been questioned by many investigators.[35-39] In general, LEED has been found to be insensitive to small amounts of impurities, or to amorphous films.[37] This, however, is not generally true of field emitters, and with the simultaneous deposition on a tungsten field emitter and a flat macroscopic single crystal, errors due to the presence of surface impurities can be minimized.

Surface reconstruction is a phenomenon observed in many adsorbate-substrate systems.[7] This occurs when the presence of some adsorbate on the selvedge layers may cause transformations in cell parameters and atomic positions. This phenomenon is observable with LEED and is important in any adsorbate-substrate system.

Recent developments in many-body, problem theories[43,44,45] have led Bauer[16] to conclude that there is no significant difference between electron scattering by light atoms and by heavy atoms. This has been shown by detailed calculations for Al and W.

EXPERIMENTAL

In the present study boron was introduced as BI_3 into the field emission chamber through an ultra-high-vacuum (UHV) variable leak valve. Boron triiodide was chosen because (a) its high vapor pressure provides a means of transporting boron to the tungsten substrate at relatively low temperatures, (b) its availability in high

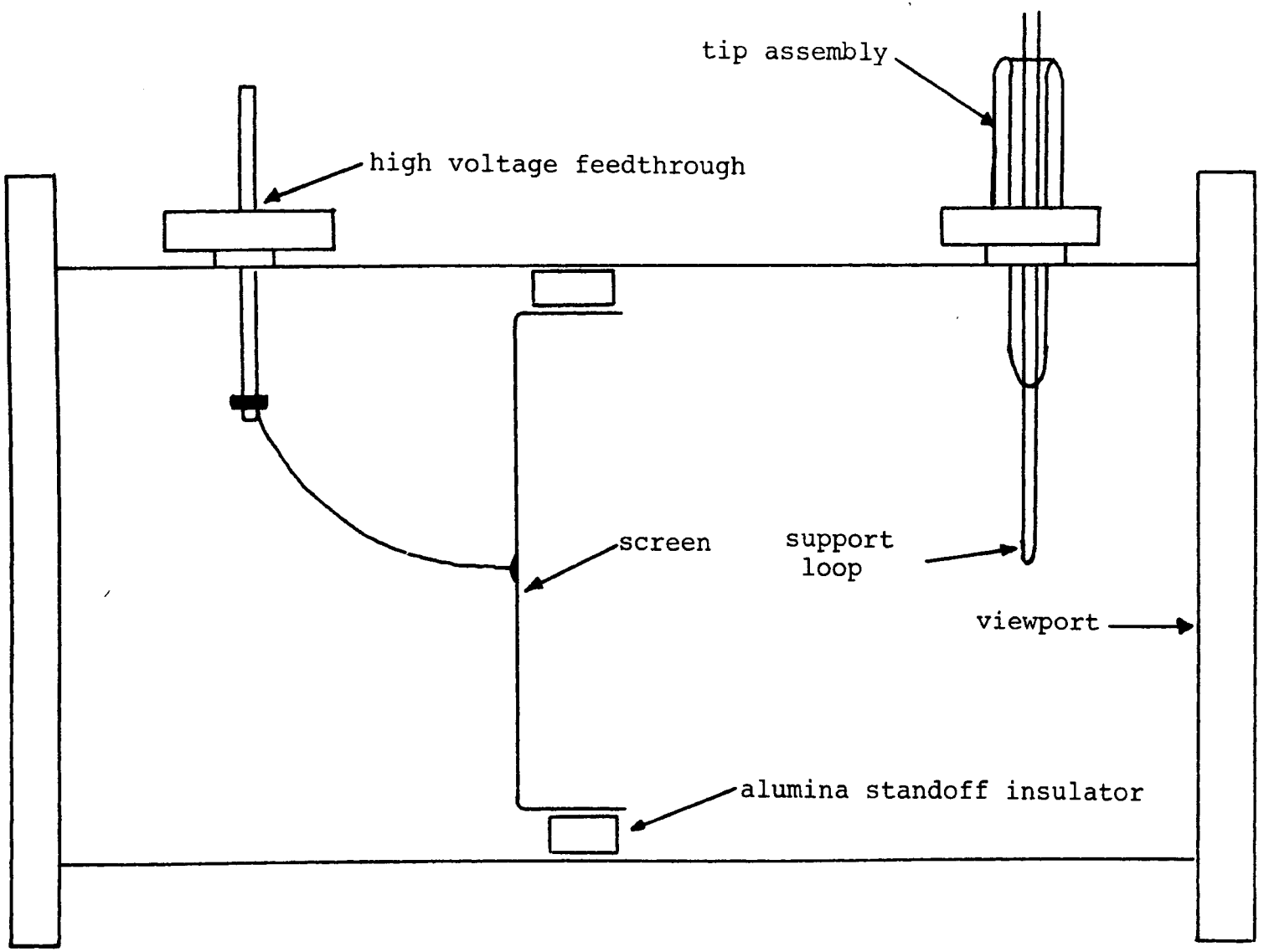

FIGURE 1. FIELD EMISSION CHAMBER

purity (99.9999%), and (c) it thermally decomposes above 450°C.

The field emitter tips were made of GE 218 tungsten wire. The tip was imaged on an inverted-view screen. This screen is unusual in that it allows direct observation of the tip and support loop through a five and three-eights inch clear-view, ultra-high-vacuum viewport. The screen was made from a stainless steel flat-bottom cup, settle-coated with a calcium tungstate phosphor. The screen was isolated from the field emission chamber by alumina standoff insulators, Fig. 1.

The tip was heated by passing ac current for Joule heating through the support loop. A Variac was used to provide flashing current and a current-regulated, ac-filament power supply was used to provide heating current for deposition sequences. The temperature of the tip was measured in two ways. An optical pyrometer was used to measure flash temperatures and a tungsten 6% rhenium-tungsten 26% rhenium thermocouple was used for lower temperatures. A comparison of these two techniques showed agreement to within 10%. The emission current was measured using a Keithly 610CR solid state electrometer.

The physical lay-out of the vacuum chamber, ion bombardment gun, LEED optics, and crystal manipulator has been described previously,[30] with the exception that the field emission chamber shown in Fig. 1 has been added in the position where the radioactive tracer gun was pre-

viously.

This physical arrangement allowed simultaneous deposition on both the field emitter and the LEED single crystal.

The LEED single crystal was prepared with standard metallographic techniques. The LEED crystal was heated by an ac, current-regulated power supply. The sample temperature was measured with an optical pyrometer and corrected for the spectral emissivity of the sample.

The high-purity BI_3 was obtained through the courtesy of the Eagle-Picher Laboratories of Miami, Oklahoma. In order to introduce the BI_3 into the UHV chamber, it was contained in frangible glass ampoules, Fig. 2. The glass ampoule was loaded into a one-piece OFHC copper jacket that also served as the gasket for sealing the input side of the variable leak. Initially, the source was prepared by pumping the chamber to $1x10^{-10}$ torr with the leak fully open. This was achieved by baking out the entire system, including the copper jacket and ampoule. The leak was then closed and the ampoule broken by crushing the copper jacket. By adjustment of the leak valve and continuous pumping with ion and sublimation pumps, the pressure of BI_3 in the chamber could be varied between $1x10^{-10}$ and $5x10^{-6}$ torr and proved stable to 1 part in 100. All field emission and LEED patterns were observed and photographed in pressures less than $1x10^{-9}$ torr, after completing a portion of a deposition

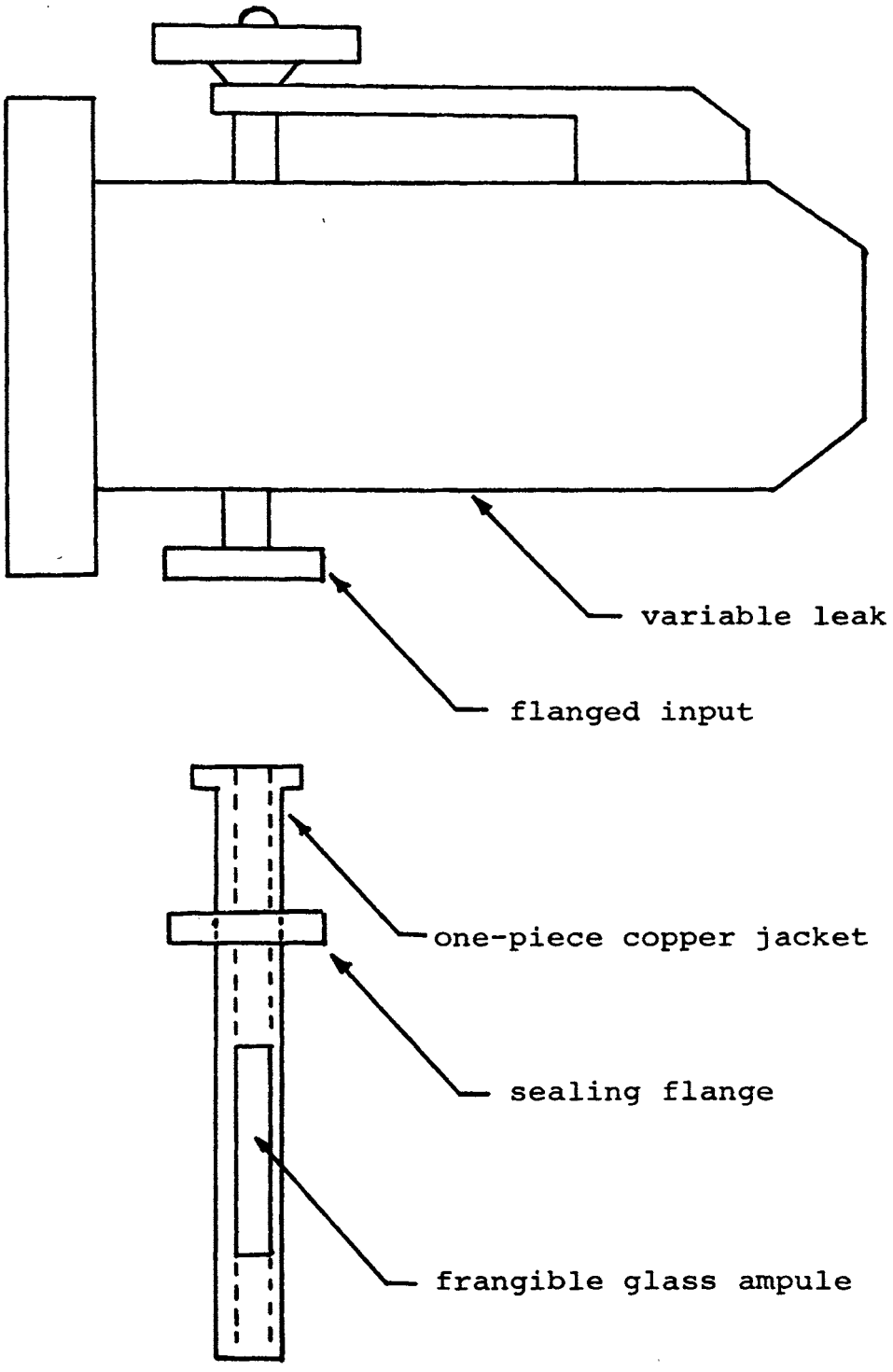

FIGURE 2. BI_3 SOURCE

sequence.

The density of boron atoms on the surface was calculated by measuring the BI_3 pressure with an ionization gauge and use of the Hertz-Knudson equation

$$J = \frac{P}{\sqrt{2\pi mkT}}$$

This method has been used previously for different adsorbates in nucleation studies.[31] Correction for the ion gauge sensitivity to BI_3 was made using a previously reported technique.[32] The sticking coefficient of BI_3 on tungsten was assumed to be unity in the temperature range 400-1500°C due to its 10+Kcal/mole heat of adsorption.[3,33,54] A plot of molecular flux vs. indicated gauge pressure is given in Fig. 3. This plot has been made using the estimated relative sensitivity of 6.5 for BI_3 as compared to N_2.

The field emitters were cleaned by flashing to temperatures >2800°K in UHV. This process gives an easily recognizable clean tungsten, field emission pattern.[34] The LEED crystals were cleaned by: (1) flashing the crystal to 2500°K, (2) exposing the crystal at 1750°K to 5×10^{-6} torr O_2 for 3 min, (3) flashing the crystal to 2500°K in UHV. This process provides a clean tungsten substrate.[6,21] To avoid the possibility of carbon out-diffusion during deposition sequences, the crystal was annealed at 1500°K for twenty-four hours in UHV and again cleaned with the above process. After this annealing process, no changes

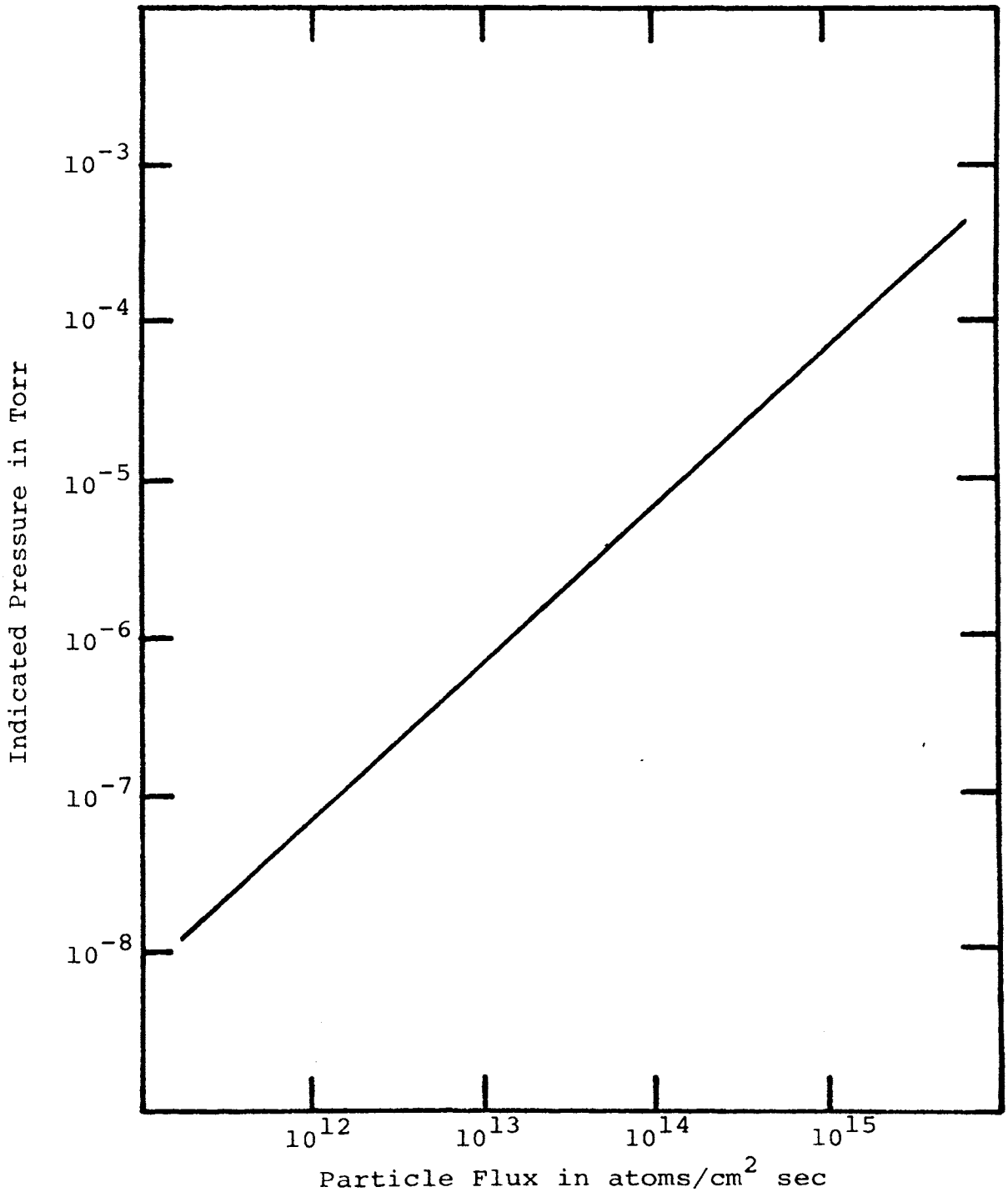

FIGURE 3. INCIDENT FLUX VS INDICATED GAUGE PRESSURE

in the LEED pattern were observed after 1 hr. of heating the crystal to the deposition temperatures studied.

RESULTS AND DISCUSSION

Deposition sequences have been observed on clean tungsten field emitter tips at several temperatures. Figures 4-14 show typical significant pattern changes due to boron adsorption at 1070°C, 975°C, 900°C, 815°C, 725°C and 375°C. Average final coverages and deposition temperatures are as indicated.

Significant changes occur on the (100), (211), (110), (332) and (334) planes. Location of planes can be found by referring to Fig. 16, a standard (110) cubic projection.

Around the (100) plane, complete darkening occurs at all temperatures studied, at $1x10^{16}$ atoms/cm^2. This coverage corresponds to about 1-2 monolayer on this area of the tip when geometrical considerations are made for the density of ledge, kink and terrace sites on the planes in this region (See Appendix II).

For the present purposes, a monolayer is defined to be the coverage required to saturate all of the most favorable substrate adsorption sites with a layer one atom thick. Note that this is less than the number which could be close packed on a flat surface. The average value of monolayer coverage for boron over a field emitter tip is 10^{16} atoms/monolayer. All coverages given will refer to

Figure 4. Boron adsorption at 1070°C

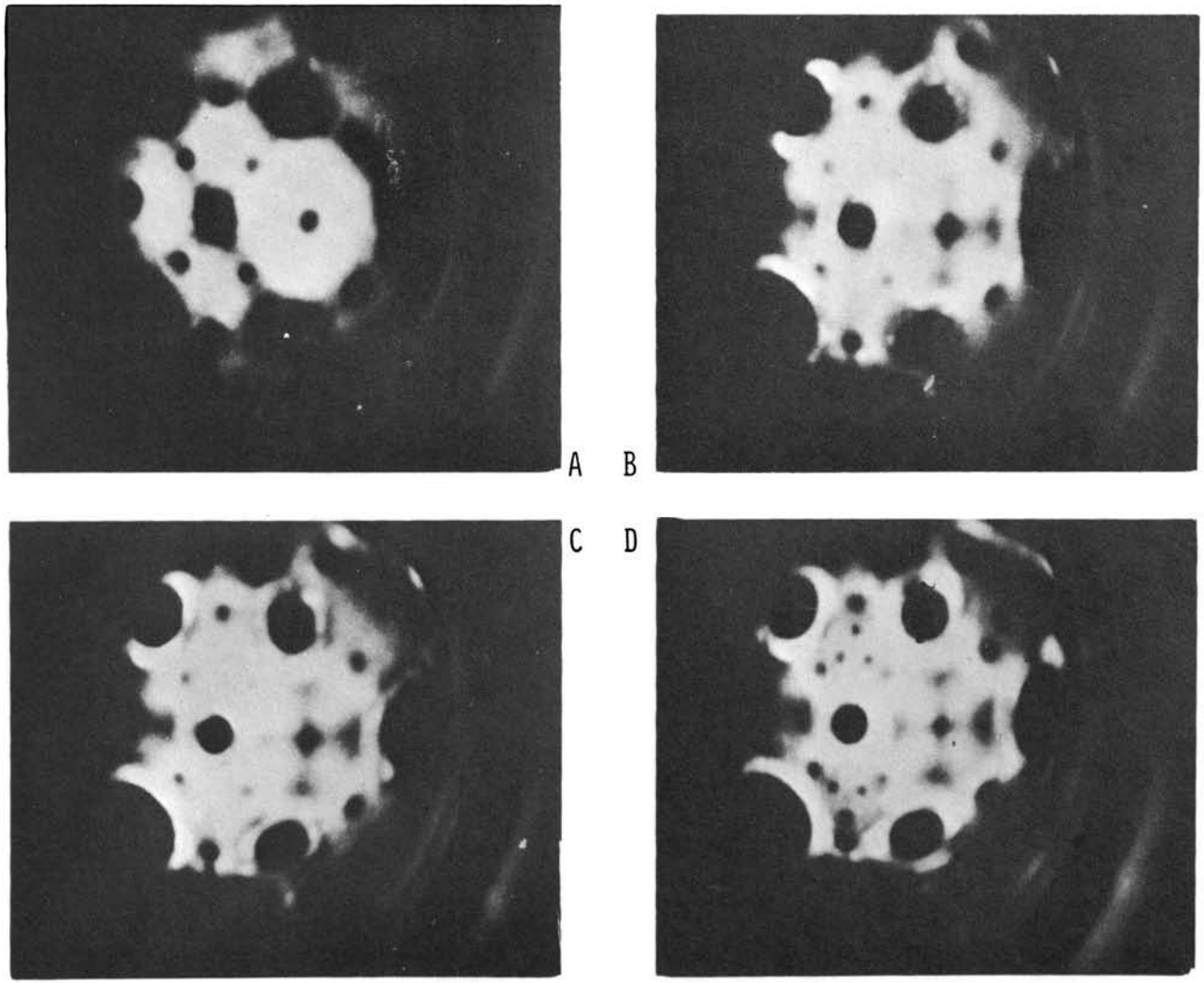

TIP TEMPERATURE 1070°C

FIGURE 4.

Figure 5. Boron adsorption at 1070°C (cont'd)

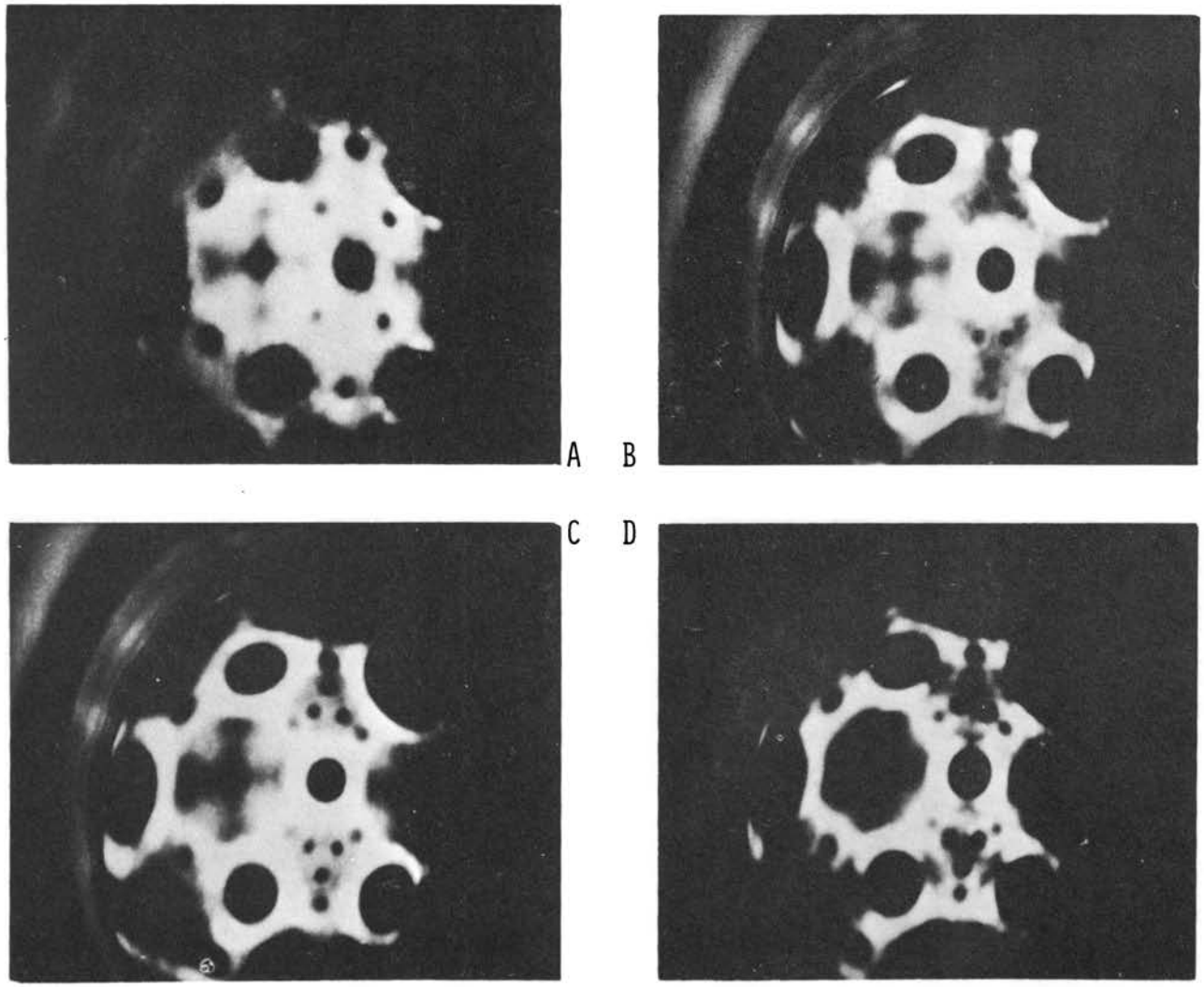

TIP TEMPERATURE 1070°C

FINAL COVERAGE 9.0×10^{16} ATOMS/CM^2

FIGURE 5.

Figure 6. Boron adsorption at 975°C.

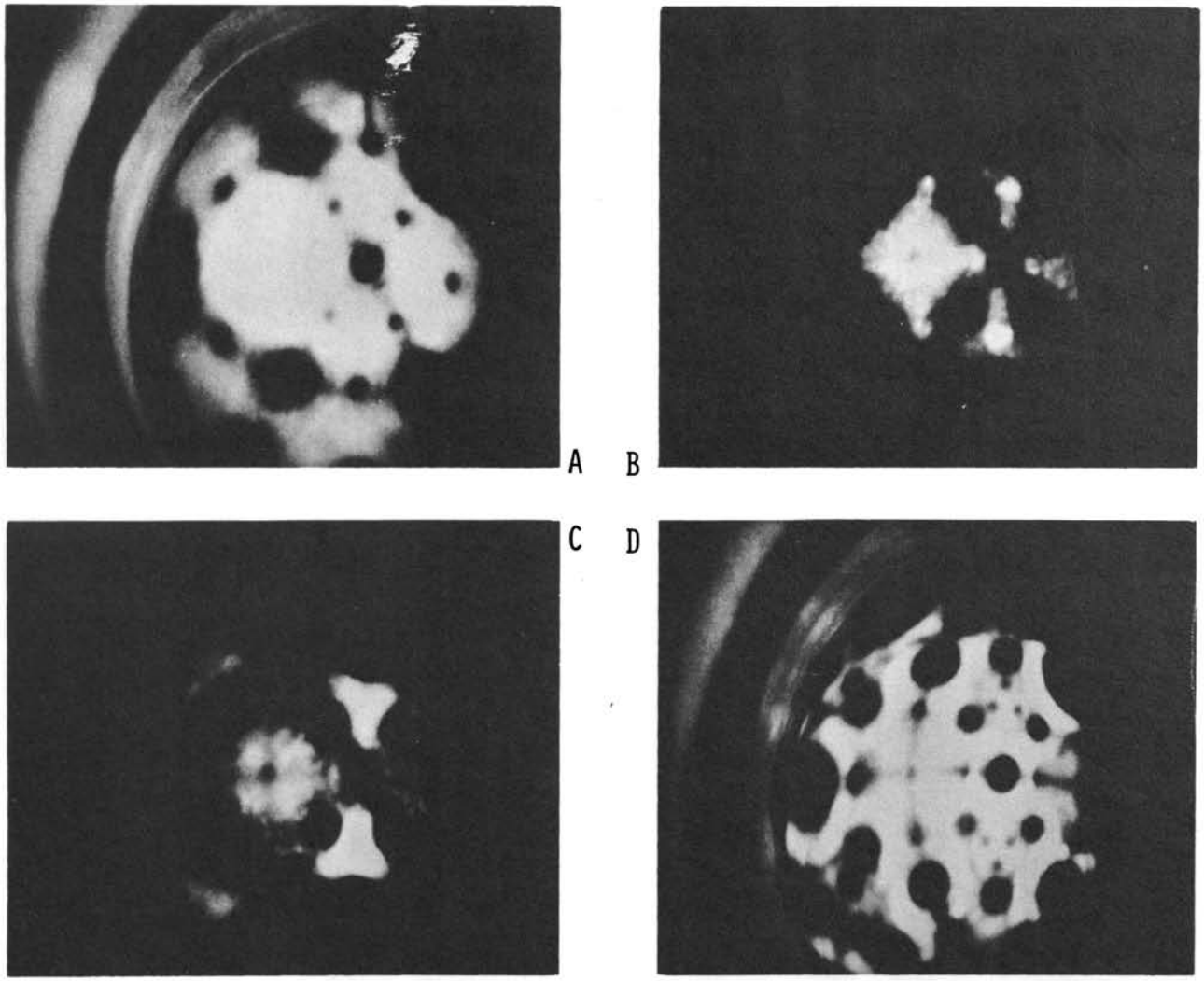

FIGURE 6.

TIP TEMPERATURE 975°C
FINAL COVERAGE 9.9×10^{16} ATOMS/CM^2

Figure 7. Boron adsorption at 900°C.

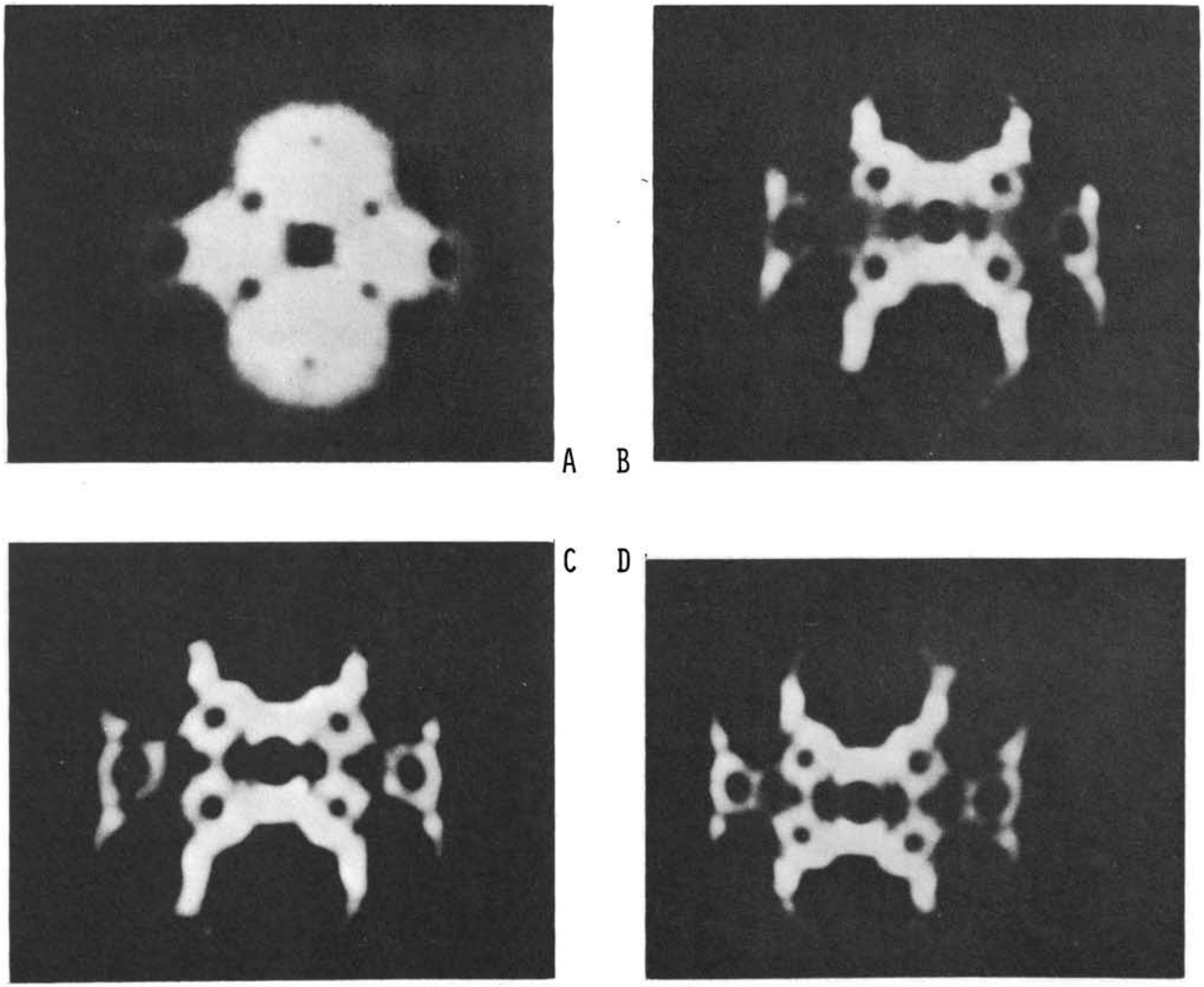

TIP TEMPERATURE 900°C

FIGURE 7. FINAL COVERAGE 1.5 x 10^{17} ATOMS/CM^2

Figure 8. Cleaning sequence from 900°C.

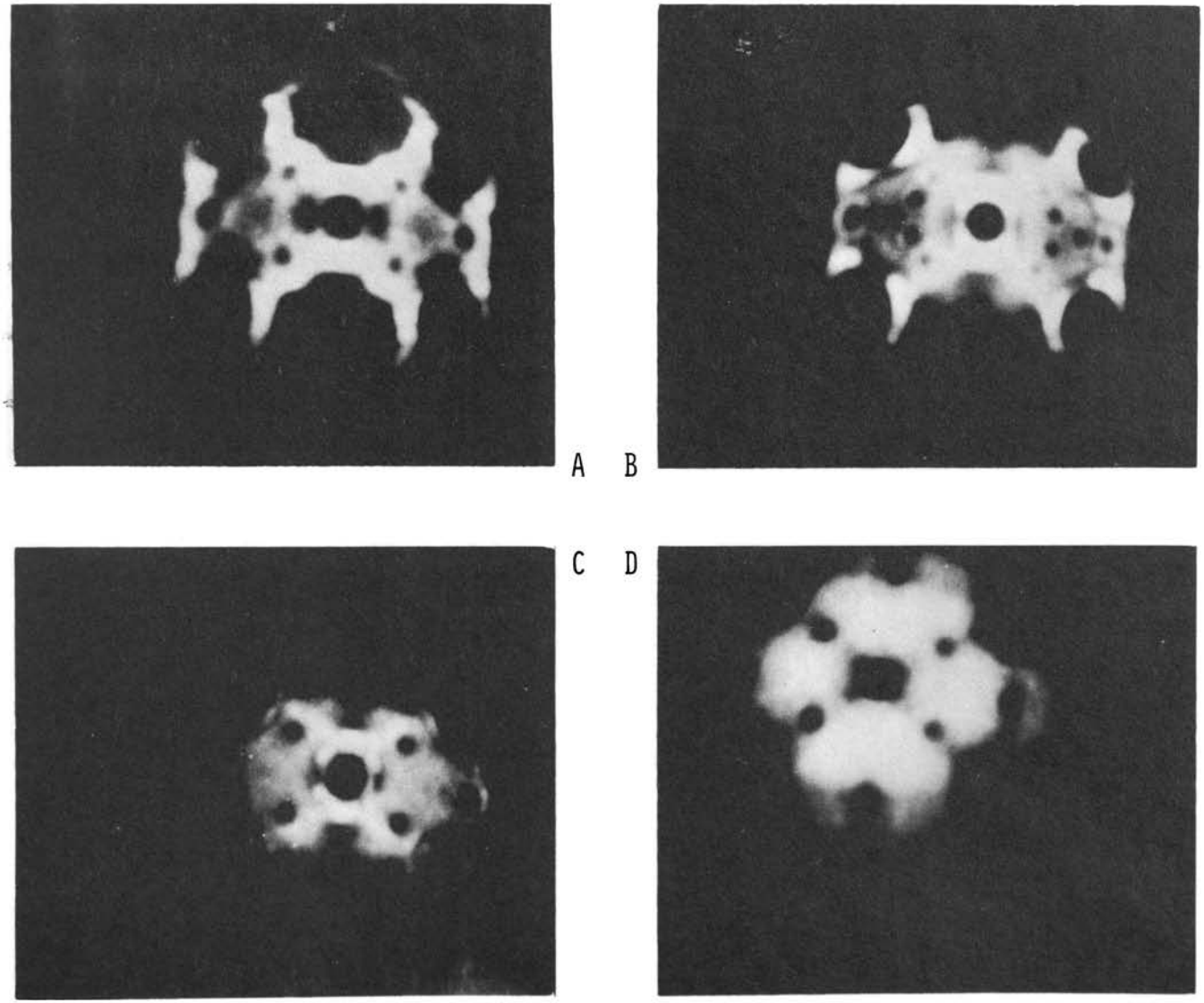

FIGURE 8. CLEANING SEQUENCE FROM 900°C

Figure 9. Boron adsorption at 815°C.

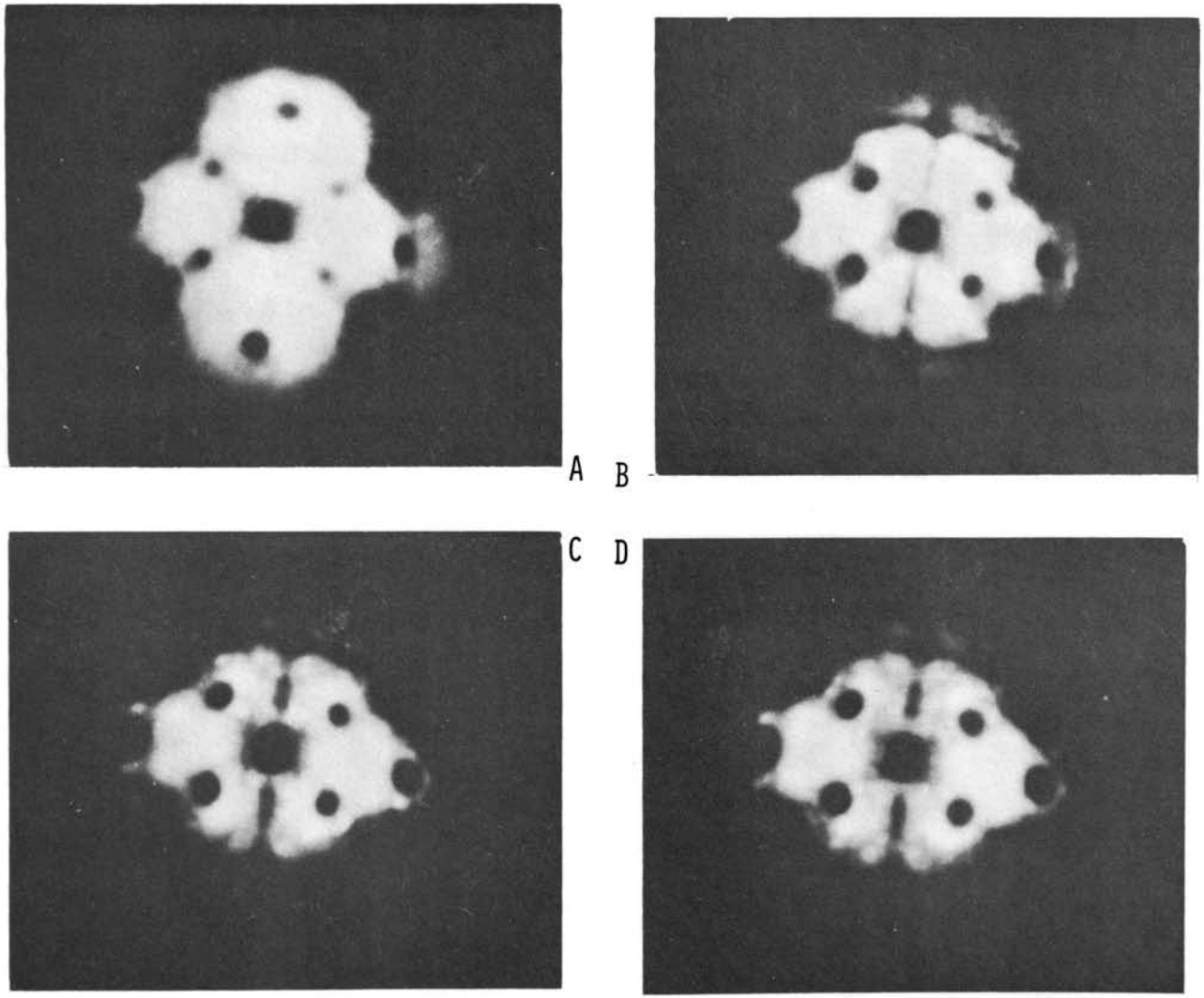

FIGURE 9. TIP TEMPERATURE 815°C

Figure 10. Boron adsorption at 815°C (cont'd).

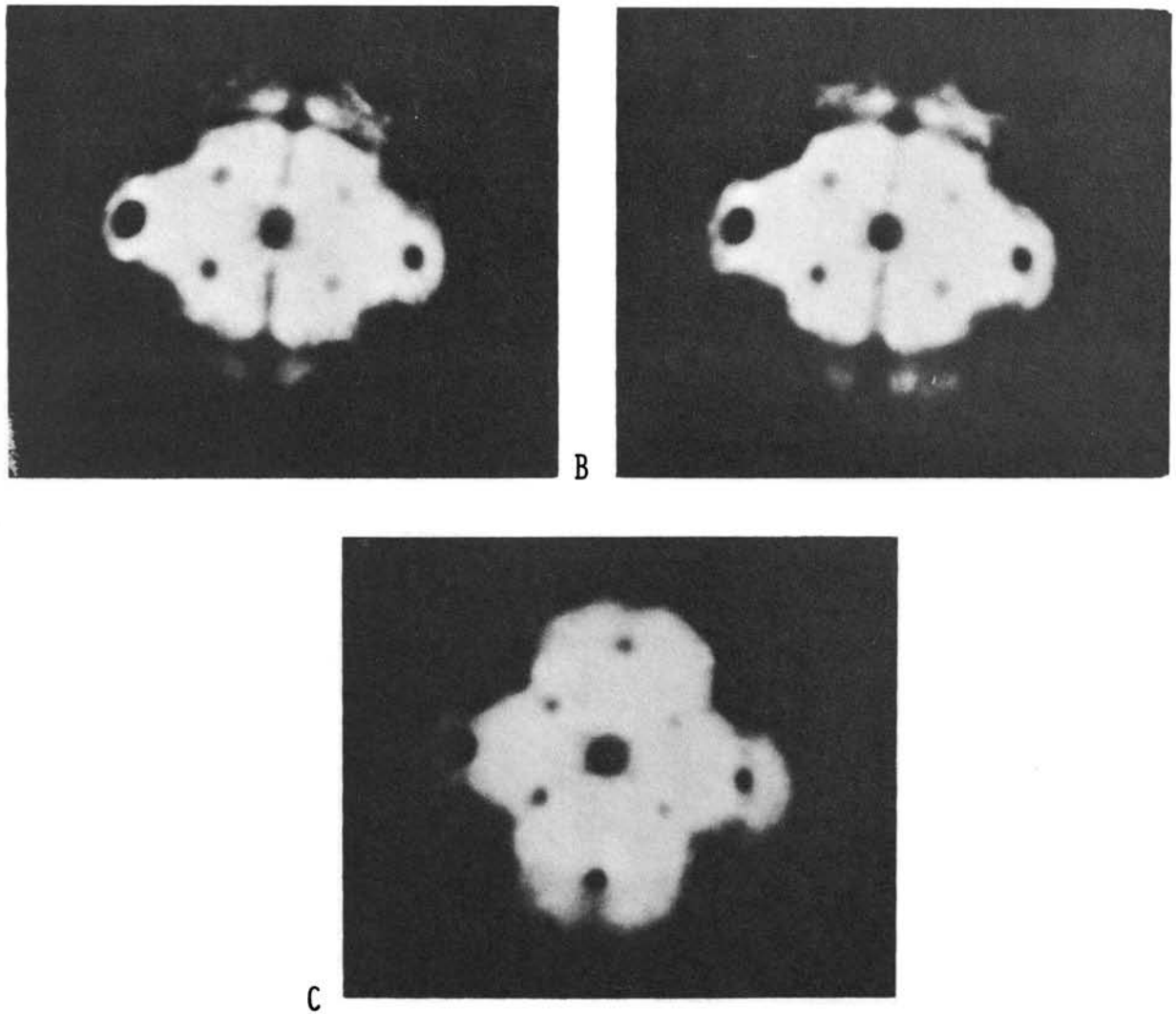

FIGURE 10.

TIP TEMPERATURE 815°C
FINAL COVERAGE 3.15×10^{15} ATOM/CM^2

Figure 11. Boron adsorption at 725°C.

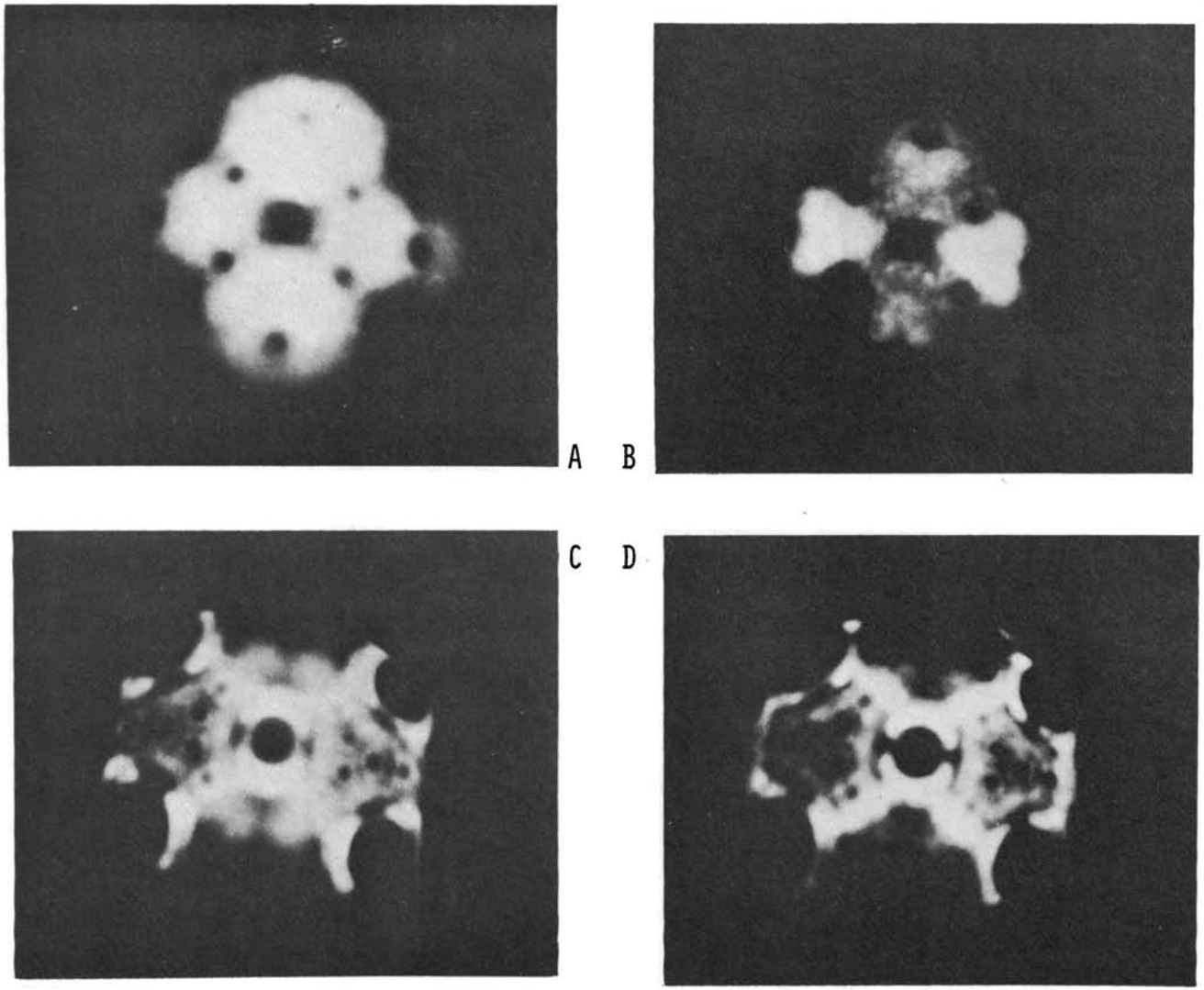

FIGURE 11. TIP TEMPERATURE 725°C

Figure 12. Boron adsorption at 725°C (cont'd).

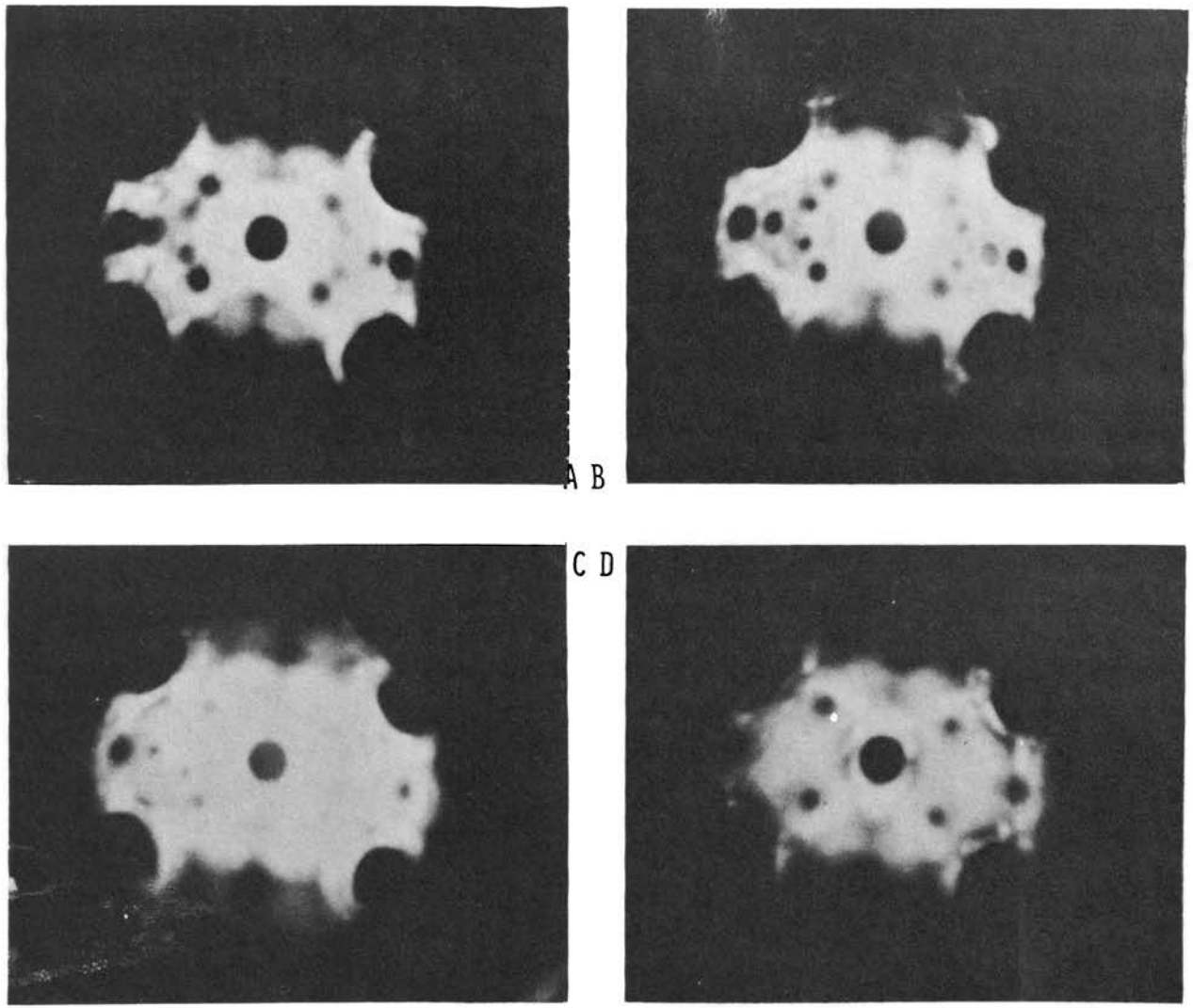

FIGURE 12.

TIP TEMPERATURE 725°C
FINAL COVERAGE 1.125×10^{16} ATOMS/CM^2

Figure 13. Boron adsorption at 675°C.

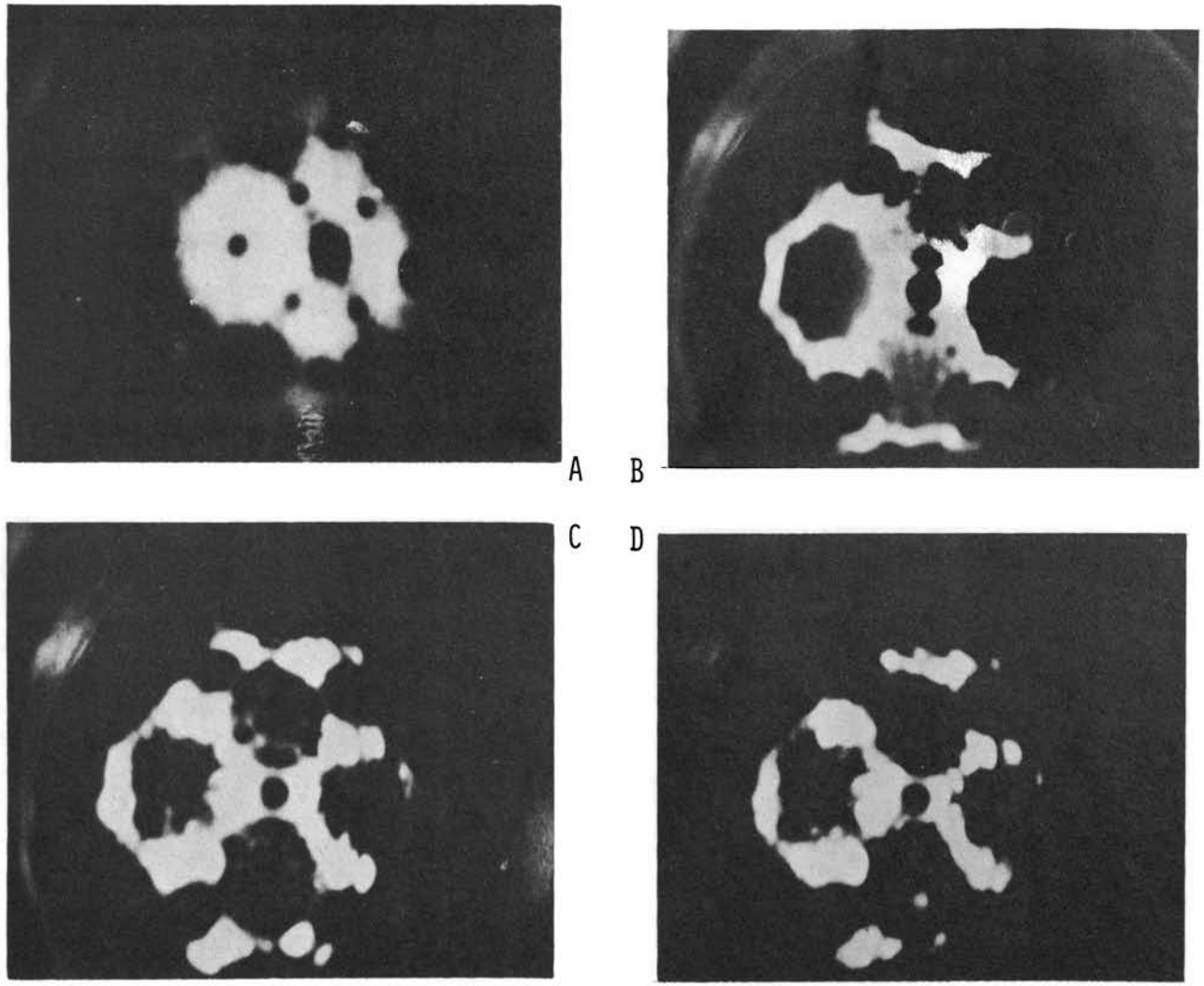

FIGURE 13. TIP TEMPERATURE 675°C

Figure 14. Boron adsorption at 675°C (cont'd).

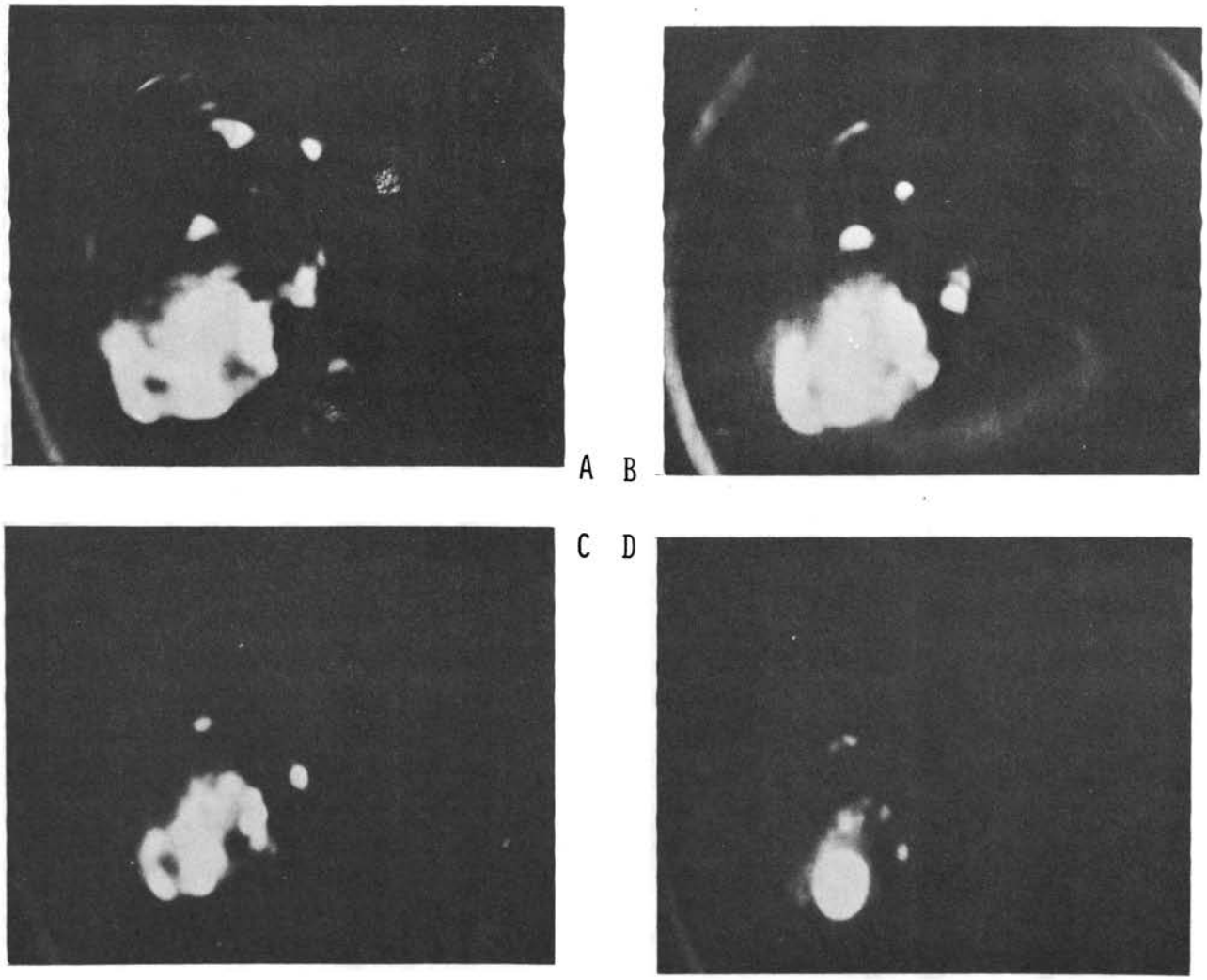

FIGURE 14.

TIP TEMPERATURE 675°C
FINAL COVERAGE 1.6×10^{18} ATOMS/CM^2

average coverages.

A possible structure for the adsorbed boron on tungsten (100) is that shown in Fig. 15. It represents a 1 monolayer coverage as defined.

The (332) and (334) planes were found to darken at low coverages, $1x10^{15}$ atoms/cm^2, for all temperatures studied.

The darkening of the (334) planes was previously thought to be a specific test for carbon,[1] but more recent work has shown that certain tungsten field emission patterns due to boron adsorption can be very similar to those produced by carbon adsorption.[3]

In this study, the development of the (334) planes was preceded by enlargement and development of the (332) planes.

On the (110) region, several interesting events were observed. At all temperatures studied, initial deposition of boron formed a bright ring of emission around the central (110) region although not completely encircling it. At temperatures above 815°C coverages as large as $2x10^{17}$ atoms/cm^2 failed to completely encircle this central (110) region. This bright ring of emission is thought to be due to the nucleation of boron in the steps around the (110) plane. At 725°C, Fig. 12 d,e, this ring of enchanced emission has completely encircled the central (110). This occurred at a coverage of $2x10^{15}$ atoms/cm^2.

Figure 15. Boron-tungsten (100) surface structure.

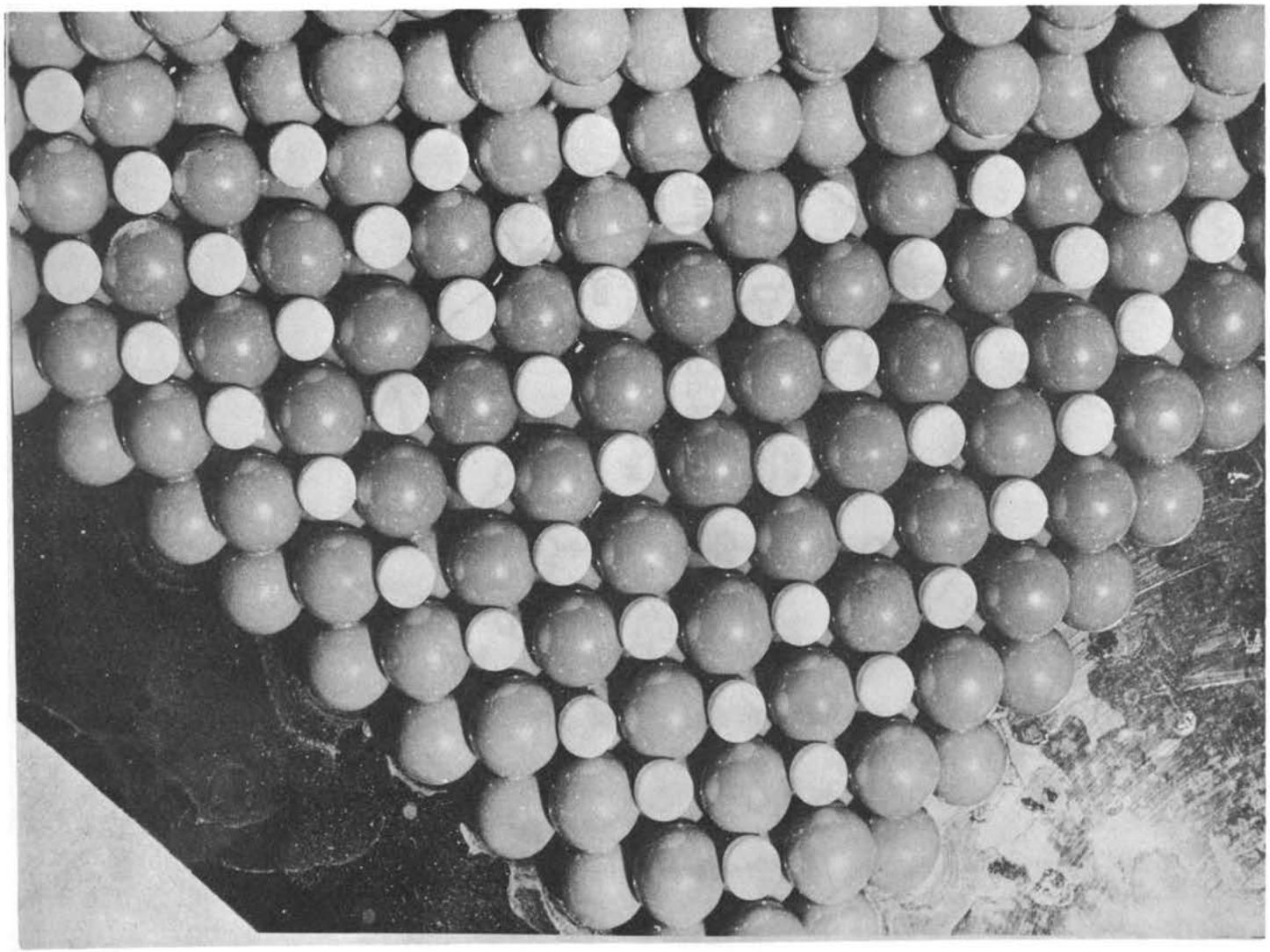

FIGURE 15.

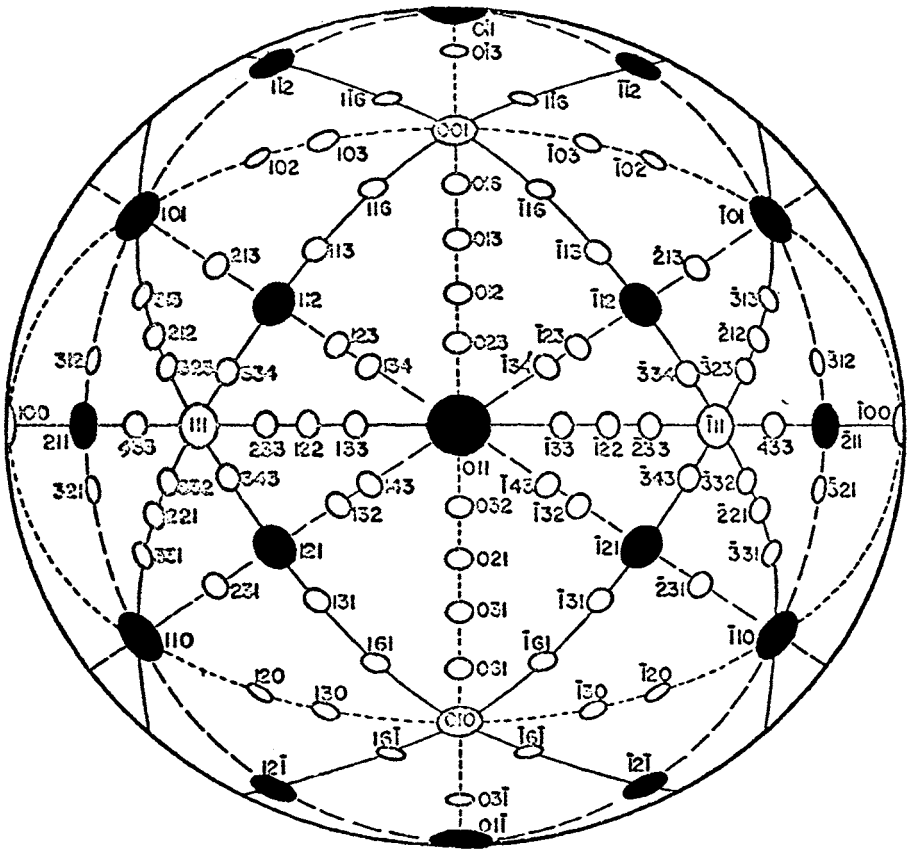

FIGURE 16. STANDARD CUBIC 110 PROJECTION

The observed fact that the complete encirclement of the (110) region will not occur at temperatures above 815°C indicates that the binding energy on a portion of the sites around the (110) region is not great enough to promote closure. At the higher temperatures, the bright ring fails to close along a line from the central (110) to the outside (211) plane, i.e. at 90° to the observed (100) region. The fact that the bright ring fails to close along this specific line may possibly be explained by the geometrical consideration that the step density along this direction is much less than in other directions. (See Appendix II).

At 675°C Fig. 13 and 14, the bright ring completely encircles the (110) plane and at an equivalent "coverage" of 1.6×10^{18} atoms/cm^2, the bright collar grows over the (110) and the pattern images as a single bright spot on the screen, Fig. 14d.

A possible explanation for this observed phenomenon is that the collar of bright emission is a torroidal, segment shaped nucleus of boron that initially forms in the steps around the (110) plane. At sufficiently low temperatures, i.e. 675°C in this study, the nucleus continues to grow until capillarity closes the central hole covering the (110) forming a spherical segment or cap-shaped, stable nucleus. The resulting nucleus has a small radius and consequently a high local field that results in emission

from this region completely overshadowing any emission from other areas of the tip.

A practical application for such a boron-modified-tungsten, field emitter tip as an electron source for electron optics is being considered.[46] Recent review articles[47,48] have shown the use of a clean tungsten, field emitter tip as a source of electrons for scanning electron microscopes. Even a clean, field emitter tip provides image intensification of one thousand times and improved resolution over conventional thermionic sources. A field emitter with a boron-covered, (110) plane similar to the pattern shown in Fig. 14D offers point source properties improved by an additional factor of 20 over that of the clean tungsten, field emitter. As atomic resolution in the SEM is approached, this factor becomes very important. However, perhaps of even greater importance are two additional advantages of this boron-modified-tungsten field source. Firstly, the modified tip is much more stable in that the tungsten surface bonds are already satisfied and the emission characteristics are not sensitive to residual gas adsorption as in the unmodified tungsten emitter case. This proves a source that can be operated at much higher pressures, i.e. it does not require UHV for stability and therefore is more practical for device applications. Secondly, the electron beam comes exclusively from a very small, centrally oriented plane with a very small divergence angle, whereas the unmodified tip is devoid of

emission from this central plane.

From this study of boron deposition on clean tungsten, field emitters it has been shown that those planes that participate in marked changes of the electron emission characteristics, are those predicted from calculations of density and the relative depth of adsorption sites. The observed time sequence of planes participating in marked, boron deposition-induced electron emission changes is in the following order: (1) (332), (2) (334), (3) (211), (4) (100), and (5) (110). See Appendix II.

Simultaneous deposition sequences were made on tungsten field emitters and a tungsten (100) single crystal at both 1000°C and 680°C.

The clean tungsten (100) LEED pattern is shown in Fig. 17. The deposition sequence at 1000°C is shown in simultaneous field emission and LEED patterns in Figures 18, 19, 20. The patterns from deposition at 680°C are shown in Figure 21.

These LEED patterns may be compared with a LEED pattern for the same tungsten crystal after exposure to oxygen in Figure 22. The similarity of the boron and oxygen on tungsten LEED patterns is quite apparent. Tucker[49] has previously commented on the similarity of the structures observed by Germer and May[50] for oxygen adsorption on the tungsten (110) plane and the structures observed for boron adsorption on the tungsten (110).[2]

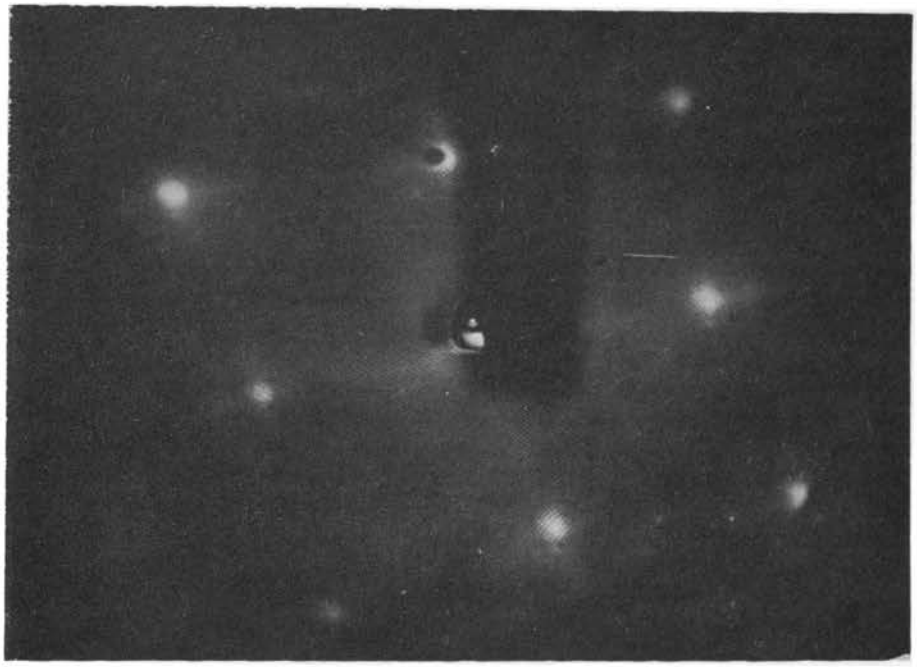

FIGURE 17. 40V CLEAN TUNGSTEN (100)

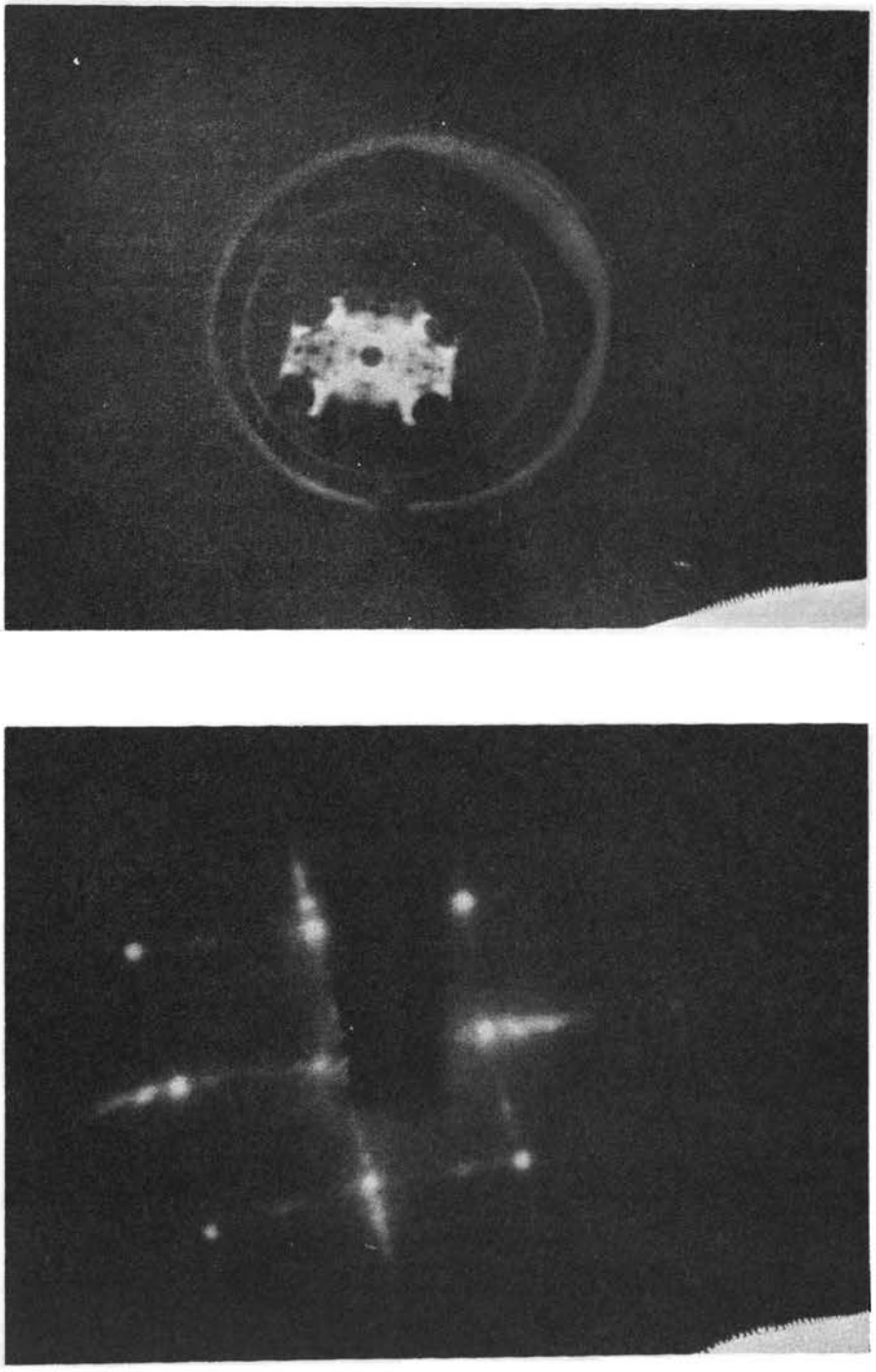

FIGURE 18. 66V W(100) 4.5×10^{12} B ATOMS/CM^2

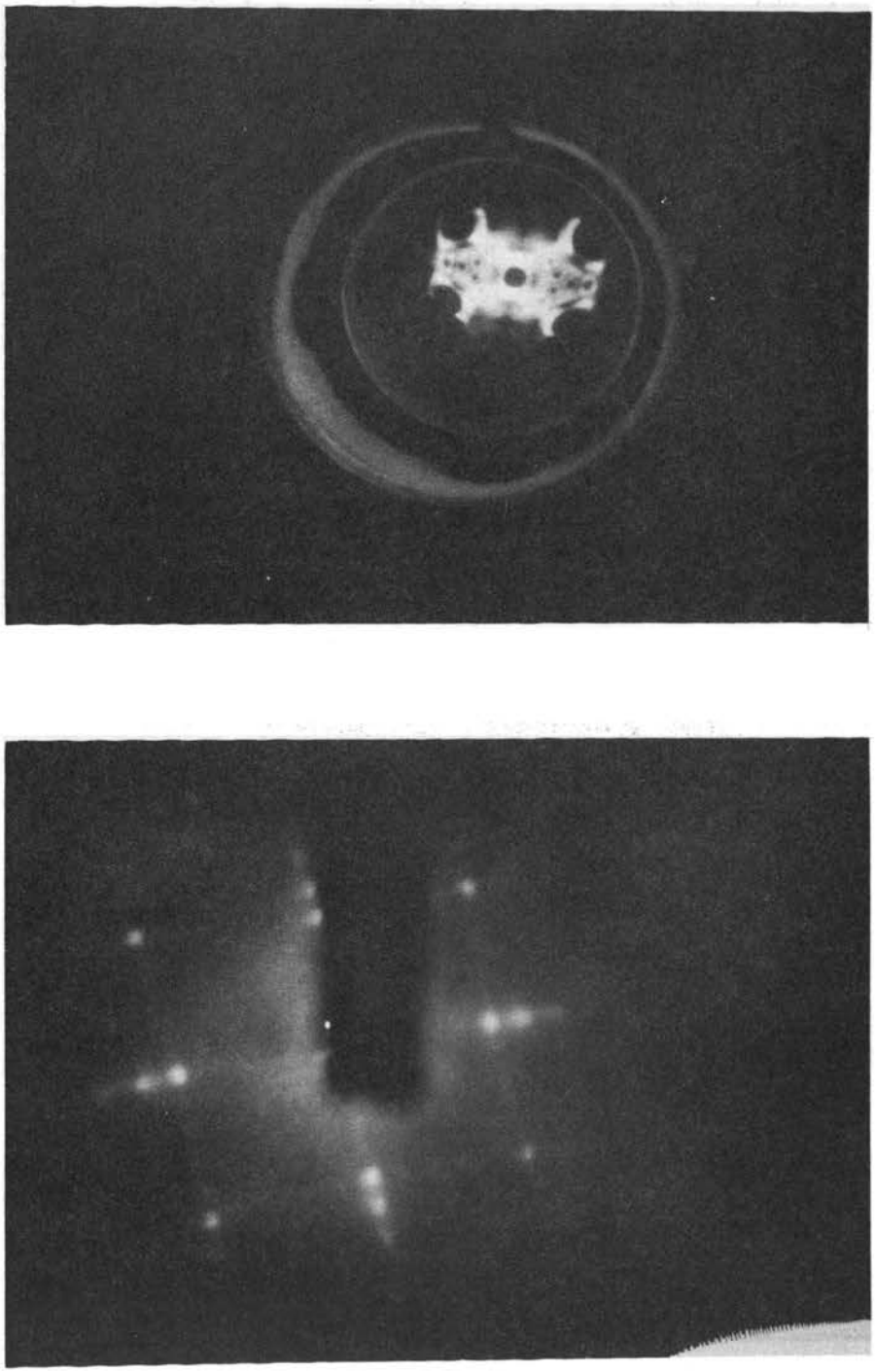

FIGURE 19. 65V W(100) 1.8×10^{13} B ATOMS/CM^2

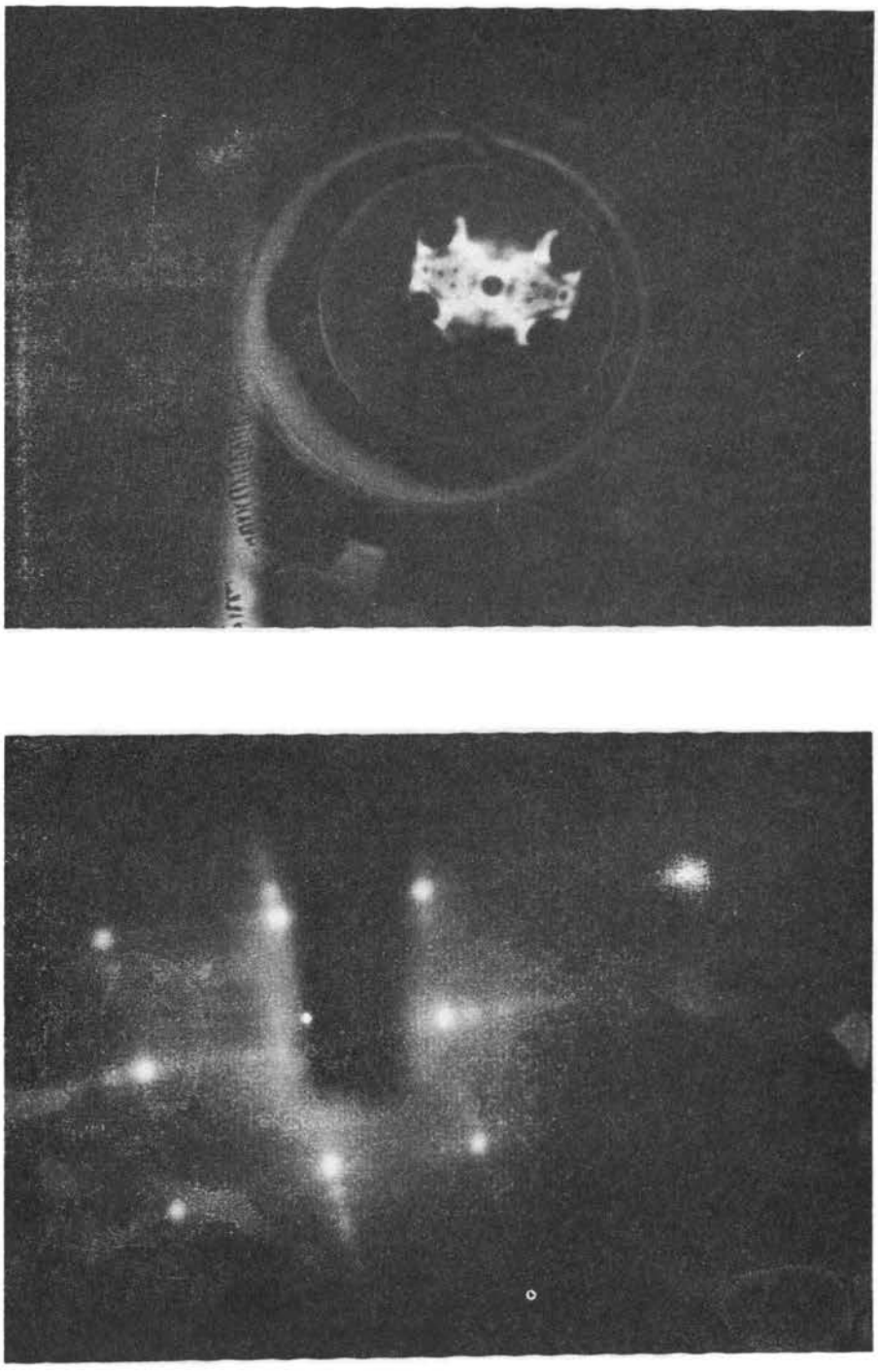

FIGURE 20. 73V W(100) 1.5 x 10^{14} B ATOMS/CM^2

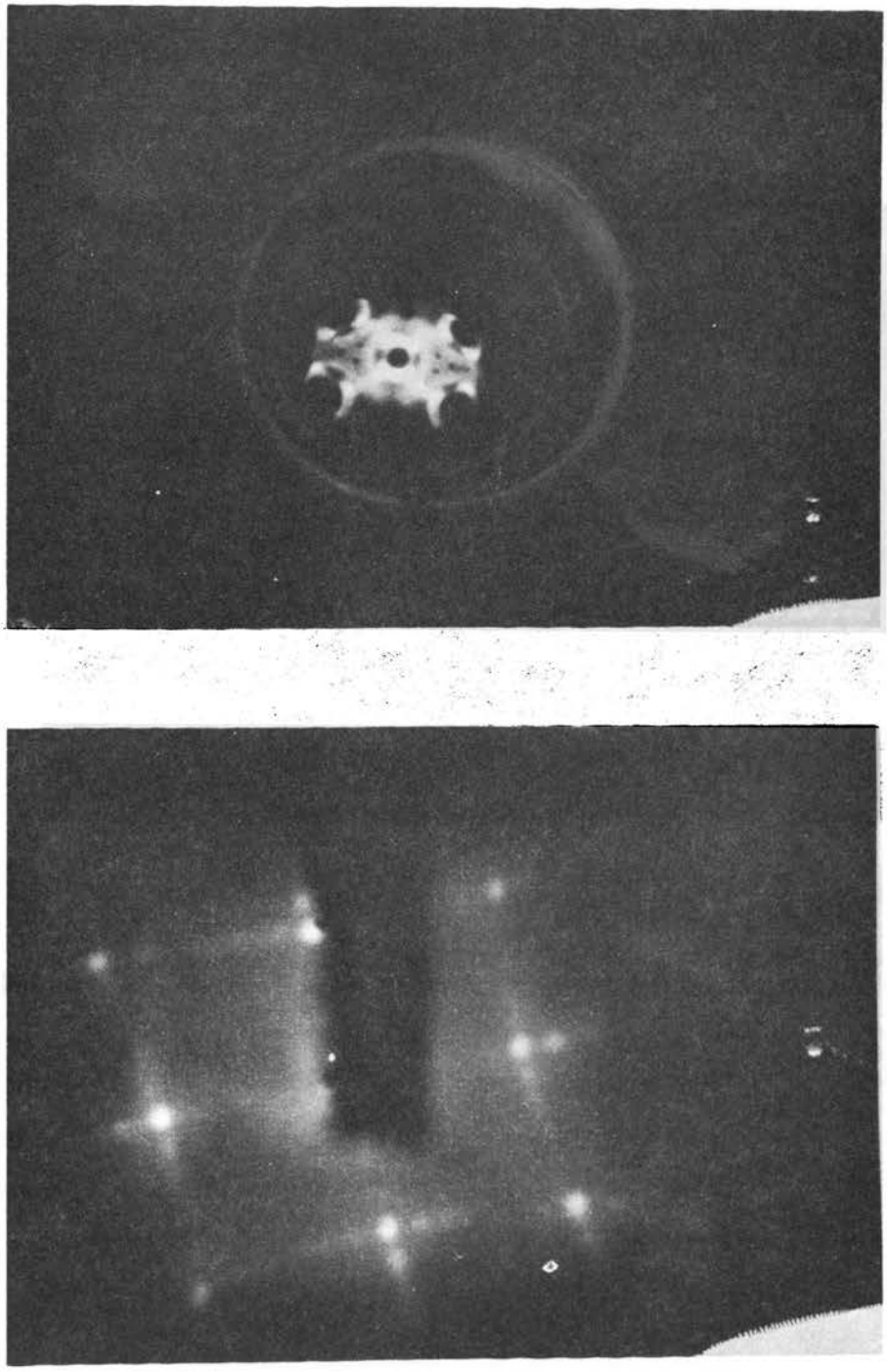

FIGURE 21. 48V W(100) 1.54 x 10^{14} B ATOMS/CM^2

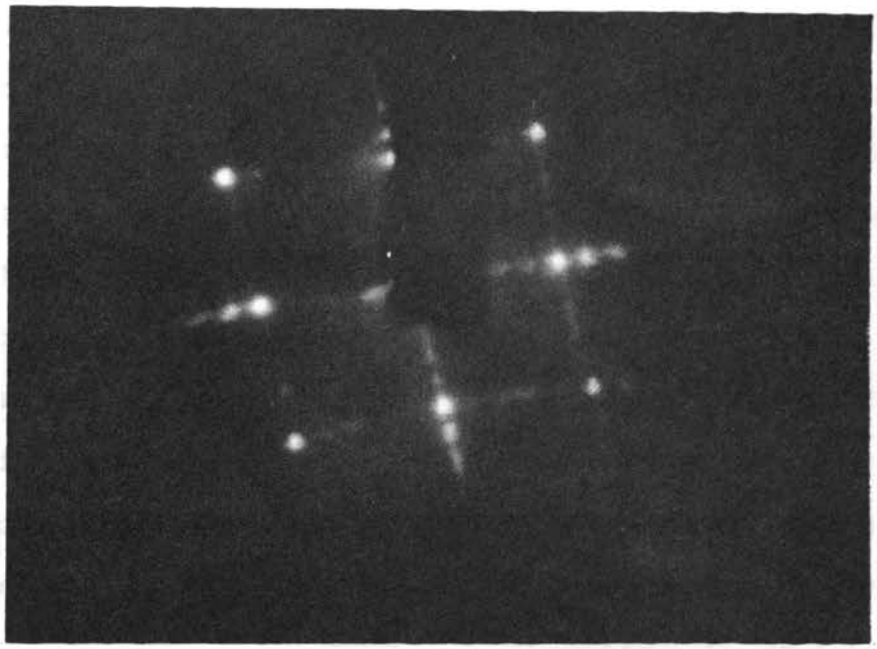

FIGURE 22. 68V W(100) 5.8×10^{13} OXYGEN ATOMS/CM^2

Application of the theory developed in Part I indicates that boron adsorption on tungsten will increase the work function at coverages between 0 and 1 monolayer. Characterization of the boron-tungsten bonding by the same theory indicates that the boron adatom will be in a negative oxidation state, thereby increasing the effective adatom radius. Thus, the boron adatom is expected to have an effective radius of 1Å when chemisorbed on a clean tungsten substrate. Therefore, boron adatoms chemisorbed on a clean tungsten (100) substrate may form an epitaxial layer, i.e. the adsorbed boron atoms may occupy those sites which represent the simplest potential minimum on a (100) tungsten substrate. These are the same sites that would be occupied by epitaxial deposition of tungsten atoms on the same clean tungsten (100) substrate.

In the present LEED studies, the results indicate that boron deposited on the tungsten (100) plane at temperatures above 650°C forms an epitaxial deposit with a slight contraction of the clean tungsten (100) surface net. Figure 15 shows this proposed structure for the boron-tungsten (100) layer at one monolayer coverage.

CONCLUSIONS

Using the extended model as developed in Part I and verified for Fowler-Nordheim field emission[52] treatments of work function changes due to adsorption, the complete

reversal of electron emission characteristics of the central tungsten (110) as observed in the field emission study cannot be explained as an effective reduction of the boron-tungsten interfacial work function. Therefore this phenomenon must be the result of the formation of a cap-shaped nucleus of boron atoms as previously postulated[3,48] (Part I). This nucleus initially forms in the steps surrounding the (110) and with further adsorption, completely covers this central (110) plane. This phenomenon is not therefore the result of the presence of a simple monolayer of boron atoms on this plane, but must be due to a local field enhancement.[53]

However, application of the same model to the tungsten (110) and adjacent regions on a field emitter tip implies that the increase in work function of this region with boron adsorption as observed in this study may be the result of a predicted increase in work function due to a strong substrate-adsorbate dipole contribution to the total work function as well as an effective increase in the local radius of curvature.

Due to the character of the adsorbate-substrate bonding of boron chemisorbed on clean tungsten (100) surfaces, the boron atom is predicted to have an effective atomic radius of 1Å at boron coverages less than 1 monolayer. Thus, chemically, vapor-deposited boron has been shown to form an epitaxial deposit on the tungsten (100) plane at coverages below 1 monolayer when adsorbed at

temperatures above 650°C.

These studies have shown that the total intensity of the LEED pattern, as observed visually and by photographic means, is unchanged due to boron adsorption on the tungsten (100) surface. This offers qualitative confirmation of the conclusions of Bauer[16] that there is no significant difference between the scattering of electrons by light atoms and by heavy atoms. Further studies of boron adsorption on tungsten with detailed intensity vs. beam energy data would be very useful in further testing these conclusions.

REFERENCES

1. R. D. Young, M.S. Thesis, Pennsylvania State University ASTIA Doc. No. 94853, Contract No. AF 18 (600) 6F2 (July, 1956).
2. C. W. Tucker, Surf. Sci., 5 (1966) 179.
3. P. D. Ownby, Ph.D. Thesis, Ohio State University (1967).
4. P. D. Ownby and R. D. Gretz, Surf. Sci., 9 (1968) 37.
5. R. H. Good and E. W. Muller, Handbook der Physik, 21 (1956) 176.
6. L. H. Germer, Sci. Am., 212 (1965) 32.
7. A. U. MacRae, Science, 139 (1963) 379.
8. J. W. May, Ind. and Eng. Chem., 57 (1965) 19.
9. C. Davisson and L. H. Germer, Phys. Rev., 30 (1927) 705.
10. W. D. Robertson, J. Vac. Sci. Technol. 8 (1971) 403.
11. N. R. Hansen and D. Haneman, Surf. Sci., 2 (1964) 566.
12. J. J. Lander and J. Morrison, J. Appl. Phys. 34 (1963) 3517.
13. E. G. MacRae, J. Chem. Phys., 45 (1964) 3258.
14. D. S. Boudreaux and V. Heine, Surf. Sci., 8 (1967) 426.
15. C. W. Tucker, J. A. P., 35 (1964) 1897.
16. E. Bauer, J. Vac. Sci. Technol., 7 (1970) 3.
17. C. B. Duke and C. W. Tucker, Surf. Sci., 15 (1969) 231.
18. K. Hrabayashi and Y. Takeishi, Surf. Sci., 4 (1966) 150.
19. E. J. Scheibner and L. N. Tharp, Surf. Sci., 8 (1967) 247.
20. J. H. Pollard, Surf. Sci., 20 (1970) 269.

21. C. C. Chang and L. H. Germer, Surf. Sci., 8 (1967) 115.

22. N. J. Taylor, Surf. Sci., 4 (1966) 161.

23. P. S. P. Wei, J. Chem. Phys., 53 (1970) 2939.

24. P. W. Palmberg and W. T. Peria, Surf. Sci., 6 (1967) 57.

25. J. J. Lander and J. Morrison, J. Appl. Phys. 34 (1963) 1403.

26. Ibid, 34 (1963) 1411.

27. J. J. Lander, Surf. Sci., 1 (1964) 125.

28. E. A. Wood, J. Appl. Phys. 35 (1964) 1306.

29. M. J. Buerger, Phase Transformations in Solids, (John Wiley and Sons, Inc., New York, 1951).

30. J. R. Wolfe and H. W. Weart, "The Structure and Chemistry of Solid Surface," Proceedings of the Fourth International Materials Symposium (John Wiley and Sons, Inc., 1969) 32-1.

31. G. M. Pound and J. P. Hirth, "Condensation and Evaporation: Nucleation and Growth Kinetics," Progress in Materials Science, Vol. II, MacMillan, New York (1963).

32. T. A. Flaim and P. D. Ownby, J. Vac. Sci. Technol., 8 (1971) 661.

33. G. Ehrlich, Advan. Catalysis, 14 (1963) 256.

34. E. W. Muller, Advances in Electronics and Electron Physics, 13 (1960) 83.

35. D. Haneman, Phys. Rev., 119 (1959) 563.

36. R. Heckingbottom, Surf. Sci., 17 (1969) 394.

37. A. V. MacRae, Surf. Sci., 4 (1966) 247.

38. F. Jona, Surf. Sci., 8 (1967) 478.

39. R. L. Park, Surf. Sci., 11 (1968) 188.

40. L. H. Germer and A. V. MacRae, J. Chem. Phys. 37 (1962) 1382.

41. A. V. MacRae, Surf. Sci., 1 (1964) 319.

42. J. J. Lander and J. Morrison, Surf. Sci., 6 (1967) 1.

43. S. M. Rose, A. Bardasis, J. Glick, D. Hone and P. Longe, Phys. Rev., 155 (1967) 379.

44. J. J. Quinn, Phys. Rev., 126 (1962) 1453.

45. J. J. Quinn and R. A. Ferrell, Phys. Rev., 112 (1958) 812.

46. P. D. Ownby, U. S. Pat. No. 3, 500, 104 Issued March 10, 1970.

47. A. V. Crewe, Sci. Am., 224 (1971) 26.

48. Industrial Research, June (1971) 21.

49. C. W. Tucker, Surf. Sci., 6 (1967) 124.

50. L. H. Germer and J. W. May, Surf. Sci., 4 (1966) 452.

51. E. P. Gyftopoulos and J. D. Levine, J. Appl. Phys., 33 (1962) 67.

52. T. A. Flaim and P. D. Ownby, Surf. Sci. (in press).

53. F. Ashworth, Advances in Electronics, 3 (1951) 1.

54. P. D. Ownby and R. D. Gratz, Surf. Sci. 12 (1968) 141.

APPENDIX I

Observations on Bayard-Alpert Ion Gauge Sensitivities to Various Gases

The pressure reading indicated by a Bayard-Alpert Ionization Gauge (hereafter BAG) at a fixed pressure is dependent upon the composition of the vapor species. A simple method of estimating the sensitivity of any BAG to a particular vapor species, without making involved absolute sensitivity measurements is greatly needed and is the subject of this letter. The ideas are taken from published literature, but have not been, to the author's knowledge, put together in the convenient form which will be shown herein.

As early as 1924, Found and Dushman[1] observed that for a particular ion gauge the absolute sensitivity to various gases varied linearly with the number of electrons in the gas phase molecule.

However, absolute sensitivity is greatly dependent upon minor changes in gauge configuration[2], i.e. grid-to-filament distance, control circuitry, etc.[3-5] Identical design BAG's with identical control circuitry and construction techniques may vary as much as 15% in absolute sensitivity[2].

Alpert[6] noted that relative sensitivity, i.e. the ratio of absolute sensitivities, should be independent of these variations, and appears to be a much more meaningful parameter to predict.

Table I shows the data available in the literature converted to relative sensitivity normalized to N_2 (nitrogen) measured in various ways by many investigators.[7]

Figure 1 shows the data plotted as a function of the number of electrons per gas phase molecule. The linearity is quite good, considering the spectrum of techniques used by the various authors.

Some scatter exists in the data for gases such as oxygen, argon and CO_2. Without attempting to justify the scatter or indicate preference to particular values, it will be noted that the linear plot through nitrogen (the reference) falls within or near the determined ranges of many vapor species over a large mass range.

Thus, the experimenter prepared with a BAG of commercial or laboratory construction and stable electronic circuitry may predict that gauge's sensitivity to various gases, and, therefore, the pressure of these gases with some degree of confidence rather than thinking only in terms of "equivalent nitrogen pressure".

Care should be exercised in using this treatment with vapor species that are known to undergo major fragmentation under electron impact, such as CH_4 and C_7H_{16} (n-heptane)[1].

While typical corrections for gauge-to-gauge variations may be of the order of 15-30%, corrections for gas phase composition are as large as 300-400% and may be easily approximated by reference to a Figure 1 type of plot.

REFERENCES

1. S. Dushman and C. G. Found, Phys. Rev. 23, 734 (1924).

2. P. A. Redhead, J. Vac. Sci. Tech. 6, 848 (1969).

3. J. Ishikawa, Japan. J. Appl. Phys. 4, 461 (1965).

4. W. D. Davis, J. Vac. Sci. Tech. 5, 23 (1967).

5. P. A. Redhead, J. Vac. Sci. Tech. 4, 57 (1966).

6. D. Alpert, J. Appl. Phys. 24, 7 (1953).

7. (a) S. Dushman and A. H. Yong, Phys. Rev. 68, 278 (1945).

   (b) S. Wagner and C. B. Johnson, J. Sci. Instr. 28, 278 (1951).

   (c) G. J. Schulz, J. Appl. Phys. 28, 1149 (1957).

   (d) S. Dushman, Scientific Foundations of Vacuum Techniques (New York: John Wiley & Sons, Inc., 1949).

   (e) H. Anderson, Rev. of Sci. Instr. 34;6, 703-704 (June 1963).

   (f) Varian Publication #87-400-074 (1965).

   (g) E. W. Rothe, J. Vac. Sci. Tech. 1, 66 (1964).

   (h) N. G. Utterback and T. Griffith, Jr., Rev. Sci. Instr. 37 (1966).

Figure 1. Relative gauge sensitivity vs. number of electrons per gas phase molecule.

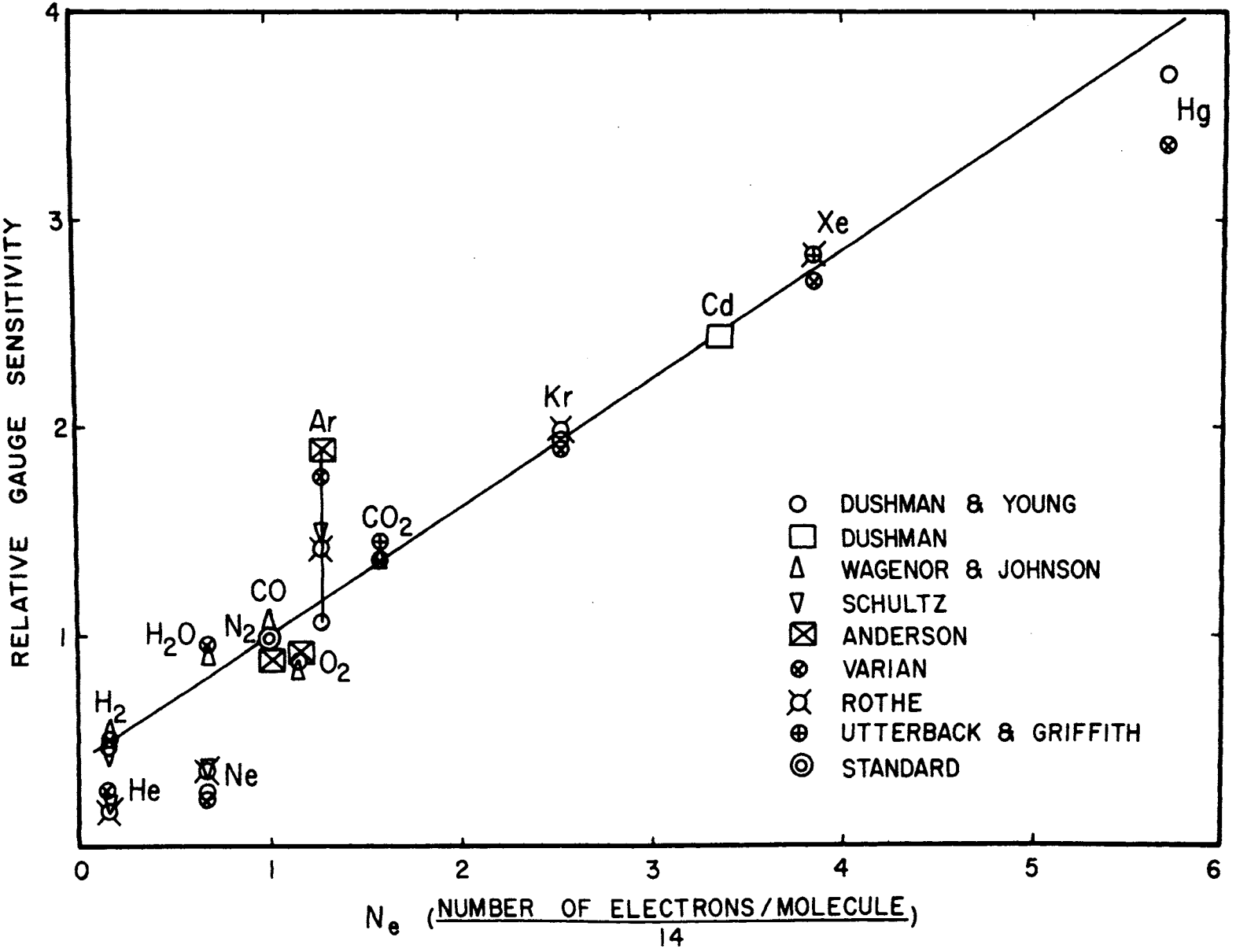
RELATIVE GAUGE SENSITIVITY
4
3
2
1
0
1
2
3
4
5
6
N_e (NUMBER OF ELECTRONS / MOLECULE / 14)
Hg
Xe
Cd
Kr
Ar
CO_2
CO
H_2O
N_2
O_2
H_2
He
Ne
DUSHMAN & YOUNG
DUSHMAN
WAGENOR & JOHNSON
SCHULTZ
ANDERSON
VARIAN
ROTHE
UTTERBACK & GRIFFITH
STANDARD

FIGURE 1

TABLE I

RELATIVE SENSITIVITY OF IONIZATION GAUGES FOR VARIOUS GASES, REFERRED TO NITROGEN AS A REFERENCE.

GAS	Dushman & Young a	Wagenor & Johnson b	Schulz c	Dushman d	Anderson e	Varian f	Rothe g	Utterback & Griffith h
H_2	0.47	0.53	0.42			.5		.422
He	0.16		0.21			.16	.182	.181
Ne	0.24		0.33			.24	.313	.312
N_2	1.0	1.0	1.0	1.0	1.0	1.0	1.0	1.00
Ar	1.19		1.5		1.89	1.78		1.42
CO		1.07			0.90	1.05		1.11
CO_2		1.37				1.37		1.43
H_2O		0.89					.90	
O_2		0.85				0.90	.82	.873
Kr	1.9					1.89	1.99	1.97
Xe	2.7					2.7	2.86	2.86
Hg	3.7					3.37		
Cd				2.4				

APPENDIX II

Calculation of Adsorption Site Densities on a Field Emitter

Consider a body-centered-cubic tungsten field emitter tip with a radius of 1000 Å. Assume the tip has hemispherical geometry, as in Figure 1.

The (110) layers are 2.238 Å apart. Call this $\bar{a} \simeq$ 2.25 Å. Assume all steps are one atom thick, i.e. 2.25 Å high. The angle between the (100) and the (110) is given by:

$$\cos \phi = \frac{h_1h_2+k_1k_2+\ell_1\ell_2}{\sqrt{(h_1^2+k_1^2+\ell_1^2)}\ \sqrt{(h_2^2+k_2^2+\ell_2^2)}}$$

$$\cos \phi = \frac{1+0+0}{\sqrt{1^2}\ \sqrt{2^2}} = \frac{1}{\sqrt{2}} = \phi_{110-100} = 45°$$

The angle between (110) - (111) is:

$$\cos \phi = \frac{1 + 1}{\sqrt{2}\ \sqrt{3}} = \frac{2}{\sqrt{6}} =$$

$$\cos \phi = .816\ \phi_{110-111} = 35.3°$$

The angle between (110) - (211) is:

$$\cos \phi = \frac{2 + 1}{\sqrt{1^2+1^2}\ \sqrt{2^2+1^2+1^2}} = \frac{3}{2\sqrt{3}} = \frac{\sqrt{3}}{2}\ \phi_{110-211}=30°$$

The angle between (110) - (310) is:

$$\cos \phi = \frac{3 + 1 + 0}{\sqrt{1^2+1^2}\ \sqrt{3^2+1^2}} = \frac{4}{\sqrt{2}\ \sqrt{10}} = \frac{4}{2\sqrt{5}} = \frac{2}{\sqrt{5}}$$

$$\cos \phi = 2/2.236 = .896 \text{ i.e. } \phi_{110-310} = 26.6°$$

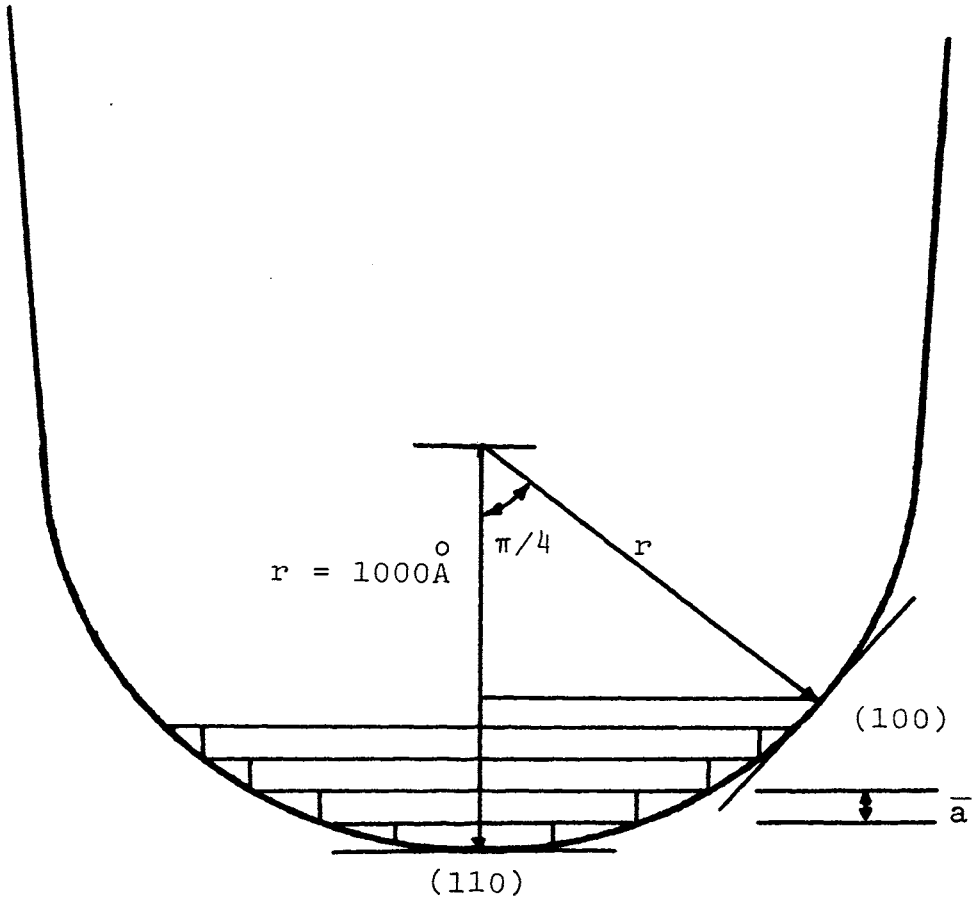

FIGURE 1. THE GENERAL FIELD EMITTER

The angle between the (110) and (100) is 45° or $\pi/4$ radius (Figure 1).

Assuming surface is a hemi-sphere, then the distance along the 100-110 zone line between (100) and (110) is given by:

$$s = r\theta$$

where s is the arc length, r is the radius of the tip, and θ is the central angle in radians.

i.e:

$$s = r\theta = 1000 \text{ Å } (\pi/4) = 250 \pi \text{ Å} = 784 \text{ Å}$$

Now, the number of one-layer high steps between the (110) and the (100) is simply (Figure 1):

$$y/\bar{a}$$

and from simple trigonometry we know that:

$$y = r - r \cos \theta = r (1 - \cos \theta)$$

i.e:

$$y_{110-100} = 1000 (1 - .707) = 293 \text{ Å}$$

$$n_{110-100} = \frac{293}{\bar{a}} = \frac{293}{2.25} = 130 \text{ steps}$$

The step density along this zone line is given by:

$$\bar{n} = \frac{n}{s} = \frac{130}{784} = \frac{1 \text{ step}}{6.02 \text{ Å}}$$

i.e. 1 step every 6.02 Å along the zone line, on the average.

The angle between the (110) and (111) is 35.3°. Therefore:

$$y = r\,(1 - \cos\theta) = r\,(1 - .816) - 184\ \text{Å}$$

$$n = y/\bar{a} = \frac{184}{2.25} = 82\ \text{steps}$$

and

$$s = r\theta = 1000\ (.612) = 612\ \text{Å along zone line.}$$

Thus the step density:

$$\bar{n} = n/s = 82/612\ \text{Å} = \frac{1\ \text{step}}{7.46\ \text{Å}}$$

i.e., 1 step every 7.46 Å along the (110) - (111) zone line. The angle between the (110) and (211) is 30.0°. Therefore:

$$y = r\,(1 - \cos\theta) = r\,(1 - .866) = 134\ \text{Å}$$

and

$$n = n/\bar{a} = \frac{134}{2.25} = 59\ \text{steps}$$

The distance between the (110) and (211) is given by:

$$s = r\theta = 1000\ (.5) = 500\ \text{Å}$$

and

$$\bar{n} = \frac{59}{500} = \frac{1\ \text{step}}{8.5\ \text{Å}}$$

i.e., 1 step every 8.5 Å.

Hence the step density along the 110-100 zone line is some 10% greater than the step density along the 110-211 zone line.

Coverages

The area of interest surrounding the (100) is essentially that bounded by four (211) planes (Figure 16).

This area is 784 Å long and 392 Å wide on a 1000 Å tip from angles previously calculated. The number of steps in this region is given by:

$$n = n_T - 2n_{110-211}$$

$$n_T = \frac{r}{a} = \frac{1000}{2.25} = 444 \text{ steps}$$

$$n_{110-211} = 59 \text{ steps}$$

$n = 444 - 2(59) = 444 - 118 = 336$ steps in this region

Assume there are two adsorption sites per a_o distance along each step. Then, there are 336 steps 784 Å long on a 1000 Å radius tip. Therefore, there are:

$$\frac{2 \times 3.36 \times 10^2 \times 7.84 \times 10^2}{3.16 \text{ Å}} = 16.65 \times 10^4$$

sites in steps on an area of

$$392 \text{ Å} \times 784 \text{ Å} = 30.7\ 10^{-12} \times \text{cm}^2$$

or, there are

$$\frac{17.44 \times 10^4}{30.7 \times 10^{-12}} = .542 \times 10^{16} \ \frac{\text{sites in steps}}{\text{cm}^2}$$

or

$$5.42 \times 10^{15} \ \frac{\text{sites in steps}}{\text{cm}^2}$$

Now on the terraces of (100) planes, there are two sites per 3.16 x 3.16 $Å^2$ of area, i.e.

$$\frac{2 \text{ sites}}{9.5 \times 10^{-16} \text{cm}^2} \quad \text{or} \quad 2.2 \times 10^{15} \ \frac{\text{sites}}{\text{cm}^2}$$

Therefore, on the region of interest there are

$$5.42 \times 10^{15} + 2.2 \times 10^{15} \frac{\text{sites}}{\text{cm}^2} \text{ or } 7.62 \times 10^{15} \frac{\text{sites}}{\text{cm}^2}$$

or approximately $1 \times 10^{16} \frac{\text{sites}}{\text{cm}^2}$ in a monolayer of boron on this region of the tip.

APPENDIX III

DIFFRACTION IN 2-DIMENSIONS

In general, a surface structure is diperiodic, which does not necessarily mean that all atoms lie in a plane, but rather that it is periodic only in two dimensions.

In diperiodic structures, the equivalent points form a two-dimensional net in which the area units are unit meshes. There are five nets analagous to the 14 Bravais lattices in triperiodic structures.

The five general unit meshes and their characteristics are given in Table 1.

Table 1

The Five Nets[1]

Name of unit mesh	Lattice Symbol	Conventional Rule of choice of axes
General parallelogram	p	a<b
Rectangle	p c	the shortest two mutually perpendicular vectors
Square	p	The shortest two mutually perpendicular vectors
120° angle rhombus	p	The shortest two vectors at 120° to each other

The five nets are shown in Figure 1

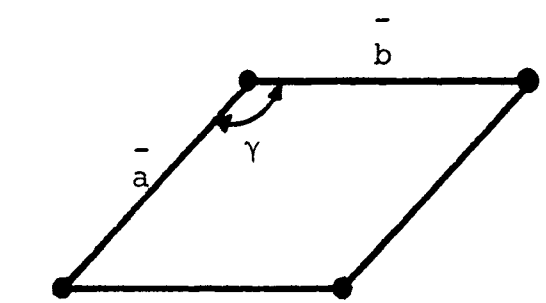

GENERAL PARALLELOGRAM

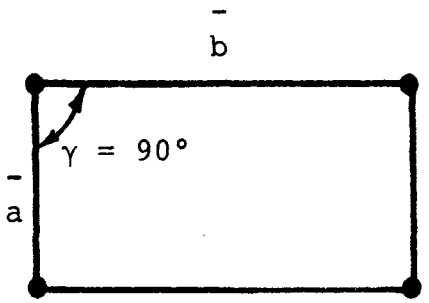

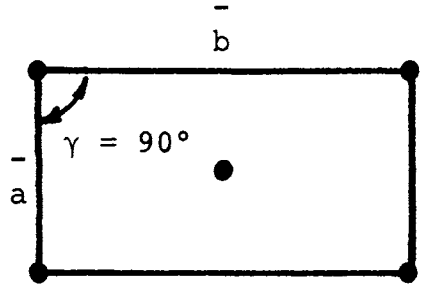

RECTANGULAR

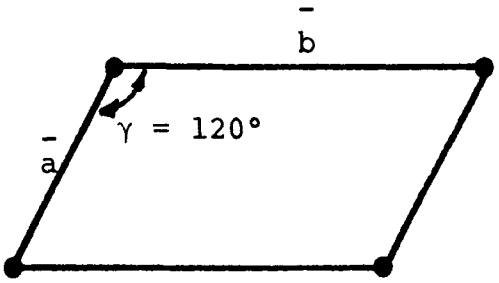

120° ANGLE RHOMBUS

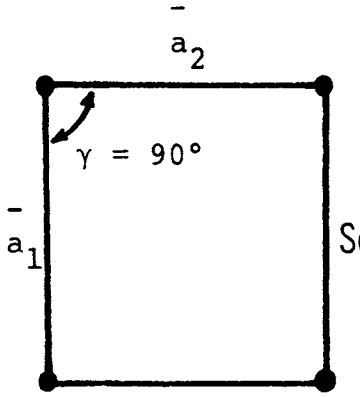

SQUARE

THE FIVE NETS

FIGURE 1

For diperiodic structures the conventional orientation of the unit mesh is with the y axis horizontal and pointing to the right, the x axis down the page, either straight or slanting to the right.

Miller indices (hk) of a set of parallel rows are the reciprocals of the row intercepts on the x and y axis; [u,v] denotes a direction where u and v are the co-ordinates of a net point (in mesh units), which with the origin, define the direction.[2]

To define the two dimensional reciprocal lattice, consider the general diperiodic lattice shown in Figure 2.

Assume this lattice is composed of particles all having the same mass and spaced at equal distances from one another along two lines intersecting at an arbitrary angle θ. The distance between particles in direction d_1 is not necessarily the same as in direction d_2. Take $\vec{d}_1$ and $\vec{d}_2$ as basis vectors drawn from the particle chosen as the origin of the lattice. The vector coordinate of any point in the lattice is then given by

$$r = \ell_1\vec{d}_1 + \ell_2\vec{d}_2 \text{ with } \ell_1, \ell_2 \text{ integers}$$

With the two basis vectors $\vec{d}_1$ and $\vec{d}_2$ for a lattice, the restriction to particles of a single type and the requirement that the particles be equally spaced along the two independent directions. The lattice described by the two basis vectors $\vec{d}_1$ and $\vec{d}_2$ is known as the <u>direct lattice</u>.

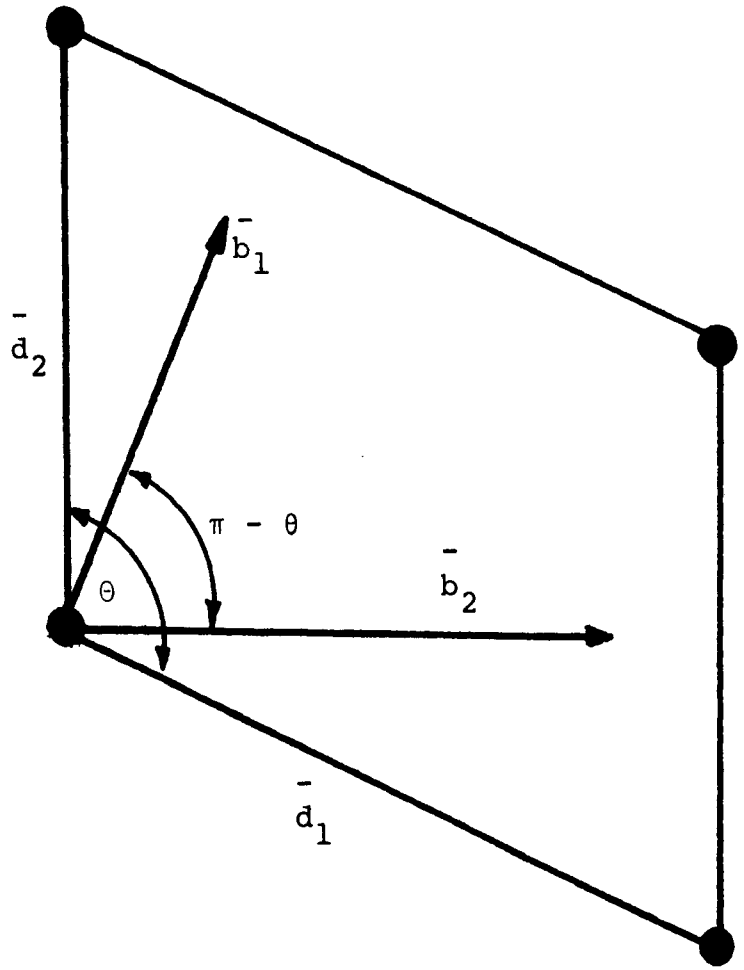

FIGURE 2. THE GENERAL LATTICE

In the derivation of the triperiodic reciprocal lattice, there are two ways of defining the reciprocal lattice. The first is to define the reciprocal lattice vectors in terms of vector products between direct lattice vectors. Thus if $\vec{d}_1$, $\vec{d}_2$, $\vec{d}_3$ are direct lattice vectors, the reciprocal lattice vectors, $\vec{b}_1$, $\vec{b}_2$, $\vec{b}_3$ may be defined by

$$\vec{b}_1 = \frac{\vec{d}_1 \times \vec{d}_2}{\vec{d}_1 \cdot \vec{d}_2 \times \vec{d}_3}$$

$$\vec{b}_2 = \frac{\vec{d}_2 \times \vec{d}_3}{\vec{d}_1 \cdot \vec{d}_2 \times \vec{d}_3}$$

$$\vec{b}_3 = \frac{\vec{d}_3 \times \vec{d}_1}{\vec{d}_1 \cdot \vec{d}_2 \times \vec{d}_3}$$

These reciprocal lattice vectors satisfy all the requisite orthogonality and reciprocity relations.

The second starting point is to define the reciprocal lattice vectors in terms of scalar products between direct lattice vectors $\vec{d}_1$, $\vec{d}_2$, $\vec{d}_3$ and reciprocal lattice vectors $\vec{b}_1$, $\vec{b}_2$, $\vec{b}_3$. Thus, $b_i \cdot d_j = S_{ij}$ $i,j = 1, 2, 3$ where S_{ij} is the familiar Kronecker delta. These two definitions have been shown to be equivalent in the triperiodic case.[3]

In the diperiodic case, the requirement that all lattice vectors lie in one plane eliminates the possibility of defining the reciprocal lattice vectors in terms of vector products between direct lattice vectors.

Thus, for each direct lattice in two dimensions, the reciprocal lattice vectors $\vec{b}_1$, $\vec{b}_2$ are defined in terms of scalar products between direct and reciprocal lattice vectors. Hence the reciprocal lattice $\vec{b}_1$, $\vec{b}_2$ vectors are defined by

$$\vec{b}_i \cdot \vec{d}_j = S_{ij} \quad i, j = 1, 2$$

and S_{ij} is the Kronecker delta.

Taking the origin of a pair of orthogonal axes x and y at the origin of the basis vectors, the vectors $\vec{d}_1$ and $\vec{d}_2$ may be written in terms of their cartesian components as follows:

$$\vec{d}_1 = (\vec{d}_{1x}\ \vec{d}_{1y})$$

$$\vec{d}_2 = (\vec{d}_{2x}\ \vec{d}_{2y})$$

or, the matrix

$$D = \begin{pmatrix} \vec{d}_{1x} & \vec{d}_{1y} \\ \vec{d}_{2x} & \vec{d}_{2y} \end{pmatrix}$$

represents the direct lattice basis system. Likewise the reciprocal lattice system has the matrix

$$B = \begin{pmatrix} \vec{b}_{1x} & \vec{b}_{2x} \\ \vec{b}_{1y} & \vec{b}_{2y} \end{pmatrix}$$

The subscripts of the elements of D must be transposed as shown for the matrix B since, if $\vec{d}_1$ and $\vec{d}_2$ are

thought of as row vectors, $\vec{b}_1$ and $\vec{b}_2$ must be column vectors as they are defined in terms of a scalar product with the direct lattice vectors.

Consider the product D·B.

$$D\ B = \begin{pmatrix} \vec{d}_{1x} & \vec{d}_{1y} \\ \vec{d}_{2x} & \vec{d}_{2y} \end{pmatrix} \begin{pmatrix} \vec{b}_{1x} & \vec{b}_{2x} \\ \vec{b}_{1y} & \vec{b}_{2y} \end{pmatrix}$$

$$= \begin{matrix} \vec{d}_{1x}\,\vec{b}_{1x} + \vec{d}_{1y}\,\vec{b}_{1y} & \vec{d}_{1x}\,\vec{b}_{2x} + \vec{d}_{1y}\,\vec{b}_{2y} \\ \vec{d}_{2x}\,\vec{b}_{1x} + \vec{d}_{2y}\,\vec{b}_{1y} & \vec{d}_{2x}\,\vec{b}_{2x} + \vec{d}_{2y}\,\vec{b}_{2y} \end{matrix}$$

$$= \begin{pmatrix} (\vec{d}_1\cdot\vec{b}_1) & (\vec{d}_1\cdot\vec{b}_2) \\ (\vec{d}_2\cdot\vec{b}_1) & (\vec{d}_2\cdot\vec{b}_2) \end{pmatrix} = \begin{pmatrix} 1 & 0 \\ 0 & 1 \end{pmatrix}$$

or $B = D^{-1}$

This implies

$\vec{b}_1$ is perpendicular to $\vec{d}_2$ and,

$\vec{b}_2$ is perpendicular to $\vec{d}_1$.

Therefore

$$\vec{b}_1\cdot\vec{d}_1 = 1 = |\vec{b}_1||\vec{d}_1| \cos(\pi/2-\theta)$$

$$= |\vec{b}_1||\vec{d}_1| \sin\theta$$

and

$$\vec{b}_2\cdot\vec{d}_2 = 1 = |\vec{b}_2||\vec{d}_2| \cos(\pi/2-\theta)$$

$$|\vec{b}_2||\vec{d}_2| \sin\theta$$

where θ is the angle between $\vec{d}_1$ and $\vec{d}_2$.

The area of the elementary cell in the direct lattice; i.e. the parallelogram with $\vec{d}_1$ and $\vec{d}_2$ for two of its sides,

is given by

$$A_d = |\vec{d}_1 x \vec{d}_2| = |\vec{d}_1||\vec{d}_2| \sin\theta$$

from elementary vector analysis. The area for the reciprocal space elementary cell is given by

$$A_b = |\vec{b}_1||\vec{b}_2| \sin\theta.$$

The product of these areas is

$$\begin{aligned} A_b \cdot A_d &= |\vec{d}_1||\vec{d}_2| \sin\theta |\vec{b}_1||\vec{b}_2| \sin\theta \\ &= \vec{d}_1 \vec{d}_2 \sin \frac{\sin\theta}{|\vec{d}_1| \sin\theta |\vec{d}_2| \sin\theta} \\ &= 1 \end{aligned}$$

i.e., the areas of the direct and reciprocal cells are reciprocals.

The notation is simplified by using $\vec{d}_1$ and $\vec{d}_2$ vectors as unit vectors defining an oblique axis system, and an arbitrary vector $\vec{r}$ is given by its ξ_1 and ξ_2 components along the $\vec{d}$ vectors,

$$\vec{r} = \xi_1 \vec{d}_1 + \xi_2 \vec{d}_2$$

and therefore,

$$\xi_1 = (\vec{r} \cdot \vec{d}_1)$$

$$\xi_2 = (\vec{r} \cdot \vec{d}_2)$$

A straight line in the plane is represented by a linear relation:

$$(\vec{a}\cdot\vec{r}) = a_1x + a_2y = c$$

or

$$a_1\xi_1 + \alpha_2\xi_2 = c$$

with

$$\alpha_1 = (\vec{a}\cdot\vec{d}_1)$$
$$\alpha_2 = (\vec{a}\cdot\vec{d}_2)$$

converseley,

$$\vec{a} = \alpha_1\vec{b}_1 + \alpha_2\vec{b}_2$$

i.e., $\vec{a}$ represents a vector orthogonal to the straight line $(\vec{a}\cdot\vec{r})$ and $c/|\vec{a}|$ is the distance δ of the line from the origin.

A direct lattice point is one with integral co-ordinates ℓ_1 and ℓ_2,

$$\xi_1 = \ell_1 \text{ and } \xi_2 = \ell_2$$
$$\vec{r} = \ell_1\vec{d}_1 + \ell_2\vec{d}_2$$

and a vector h in the reciprocal lattice is

$$\vec{h} = h_1\vec{b}_1 + h_2\vec{b}_2$$

h_1, h_2 integers

Consider

$$(\vec{h}\cdot\vec{r}) = h_1(\vec{b}_1\cdot\vec{r}) + h_2(\vec{b}_2\cdot\vec{r}) = c$$
$$= h_1\xi_1 + h_2\xi_2 = c$$

For $c \equiv o$, the line $\vec{h}\cdot\vec{r}$ passes through the origin. Other lattice rows will correspond to different c values.

To find the smallest distance between a lattice row and the origin, the smallest non-zero value of c must be found. Since h_1, h_2, ξ_1, and ξ_2 are integers, c must be an interger for a lattice row, i.e. for the closest row, $|c| = 1$.

This means that the distance between each of the lattice rows in the set (h_1,h_2) is

$$\delta = \frac{|c|}{|h|} = \frac{1}{|h|}$$

Thus, a point (h_1,h_2) in the reciprocal lattice defines a set of lattice rows in the direct lattice.

These straight rows are perpendicular to the vector

$$\vec{h} = h_1\vec{b}_1 + h_2\vec{b}_2$$

and are spaced at a distance of $1/|\vec{h}|$ from one another.

Using the above argument, similar relations are found for all rows of the direct lattice. The whole reciprocal lattice is built up of repeated translations of the reciprocal lattice basis vectors $\vec{b}_1$ and $\vec{b}_2$.

This translation produces a planar array of points, each of which is labeled with its co-ordinates in terms of the basis vectors. The extended reciprocal lattice has the following properties:

(1) A vector $\vec{h}(h_1,h_2)$ drawn from the origin of the reciprocal lattice to any point in it having co-ordinates h_1,h_2 is perpendicular to the direct lattice row whose

Miller indices are h_1, h_2.

(2) The length of the vector $\vec{h}(h_1,h_2)$ is equal to the reciprocal of the spacing δ, of the (h_1,h_2) rows, or

$$|\vec{h}_{h_1,h_2}| = \frac{1}{\delta_{h_1,h_2}}$$

To analyze the diffraction of a wave into three-dimensions by a two-dimensional lattice, the Ewald construction is quite helpful. The Ewald construction requires a true diffraction process, and for a two-dimensional lattice, a diffraction process that involves only the two-dimensional lattice.

To use the Ewald construction, the two-dimensional reciprocal lattice must be extended to three dimensions. The most general extension of a planar array of points into three dimensions is an array of parallel rods perpendicular to the planar direct lattice.

Using this extension of the two-dimensional reciprocal lattice, the Ewald construction appears as in Figure 3.

This derived model predicts continuous diffraction with continuous change of incident beam wavelength ($\lambda<d$) and continuous diffraction with continuous rotation of the direct lattice. All of these phenomenon have been observed experimentally with Low Energy Electron Diffraction.

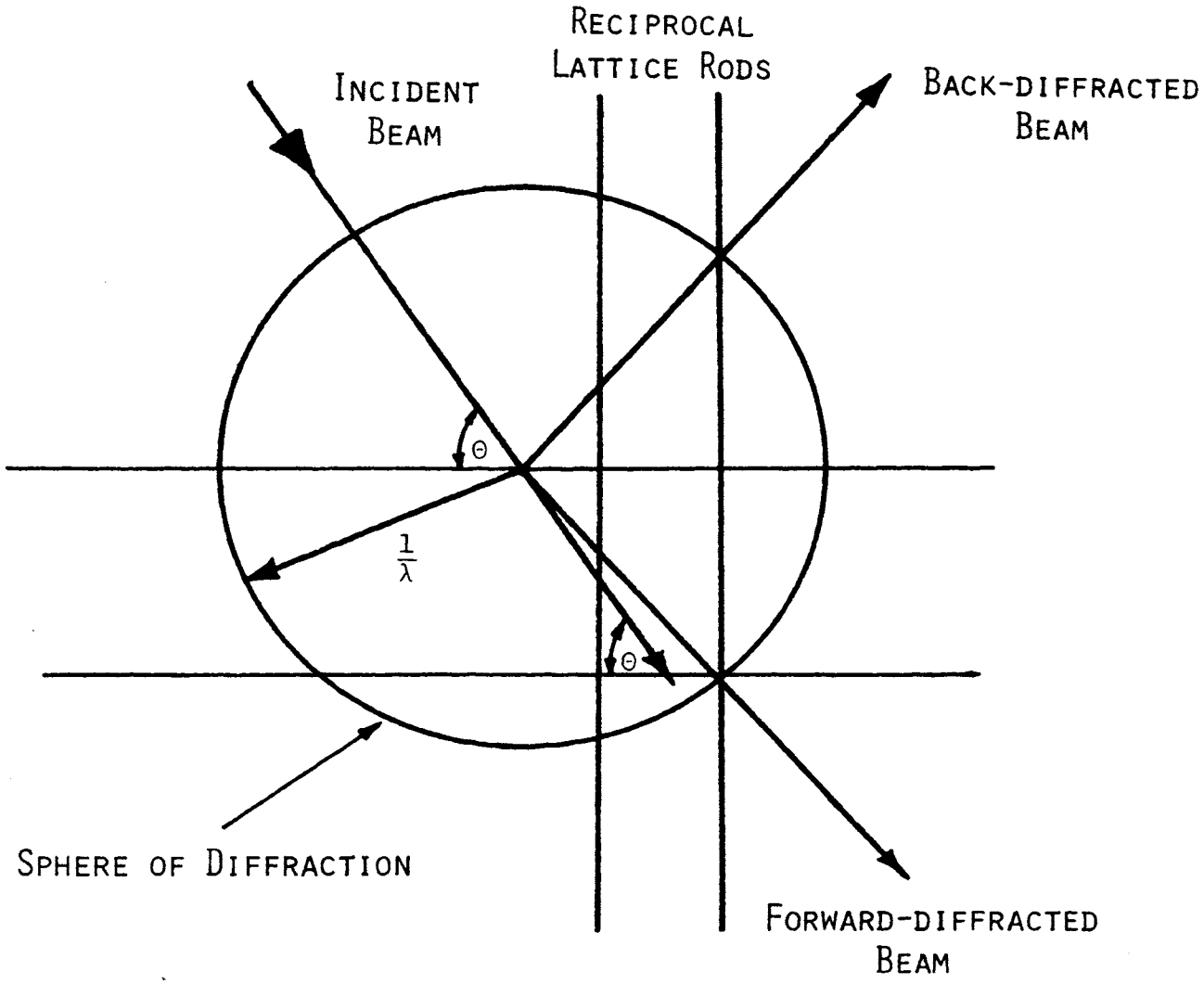

FIGURE 3. THE EWALD CONSTRUCTION

BIBLIOGRAPHY

1. International Tables for X-Ray Crystallography Vol I (Kynoch Press, Birmingham, England) (1959).

2. Wood, E. A., J. Ap. P., 35, 1306 (1964).

3. Cullity, B. D., "Elements of X-Ray Diffraction", Addison-Wesley. (1967).

VITA

The author was born in Paris, Texas, July 11, 1946. His father was a career Army officer and he attended a series of private and public schools during his elementary education. He was graduated from John F. Hodge high school in 1964. He entered the University of Missouri-Rolla in 1964 and received a B.S. degree in 1968. He entered graduate school in 1968 and has been in graduate study since that time.